Analytical and Experimental Analyses of Nonlinear Vibrations in a Rotary Inverted Pendulum

Mohammadjavad Rahimi dolatabad (mj.rahimi@kish.sharif.edu)
Sharif University of Technology - Kish International Campus https://orcid.org/0000-0003-1162-8111
Abdolreza Pasharavesh
Sharif University of Technology https://orcid.org/0000-0002-5797-5306
Amir Ali Akbar Khayyat
Sharif University of Technology - Kish International Campus

Research Article

Keywords: Inverted Pendulum, Nonlinear Vibration, Analytical models, Dynamic Stability

Posted Date: August 10th, 2021

DOI: https://doi.org/10.21203/rs.3.rs-273757/v1

Version of Record: A version of this preprint was published at Nonlinear Dynamics on January 6th, 2022. See the published version at https://doi.org/10.1007/s11071-021-06969-0.

Abstract

Gaining insight into possible vibratory responses of dynamical systems around their stable equilibria is an essential step, which must be taken before their design and application. The results of such a study can significantly help prevent instability in closed-loop stabilized systems through avoiding the excitation of the system in the neighborhood of its resonance. This paper investigates nonlinear oscillations of a Rotary Inverted Pendulum (RIP) with a full-state feedback controller. Lagrange's equations are employed to derive an accurate 2-DoF mathematical model, whose parameter values are extracted by both the measurement and 3D modeling of the real system components. Although the governing equations of a 2-DoF nonlinear system are difficult to solve, performing an analytical solution is of great importance, mostly because, compared to the numerical solution, the analytical solution can function as an accurate pattern. Additionally, the analytical solution is generally more appealing to engineers because their computational costs are less than those of the numerical solution. In this study, the perturbative method of multiple scales is used to obtain an analytical solution to the coupled nonlinear motion equations of the closed-loop system. Moreover, the parameters of the controller are determined, using the results of this solution. The findings reveal the existence of hardening- and softening-type resonances at the first and second vibrational modes, respectively. This led to a wide frequency range with moderately large-amplitude vibrations, which must be avoided when adjusting a time-varying set-point for the system. The analytical results of the nonlinear vibration of the RIP are verified by experimental measurements, and a very good agreement is observed between the results of both approaches.

1. Introduction

The stabilization and tracking control of Inverted Pendulums (IPs) implementing either linear or rotary base motions is a classical engineering problem capable of being employed as a benchmark for various control theories [1]. In this light, the underactuated control [2, 3] of these systems, exhibiting inherent nonlinearity and instability, is a challenging subject which, due to its growing application in the development of walking robots, has become the focus of much research during the recent years. Basically, the most common types of IPs are the single-arm Rotary Inverted Pendulum (RIP) [4], the double IP [5], and the cart IP [6, 7].

Because of the wide range of applications of IPs, the development of appropriate strategies and methods to control their response has become more appealing and many controllers have been, and still continue to be, tested and introduced in the last few decades. Among these controllers, the linear types are more popular because of their less computational demand to produce control signals, as well as their lower complexity. For example, Proportional-Integral-Derivative (PID) controllers, optimal controllers provided by Linear Quadratic Regulator (LQR) method, and Model Predictive Controllers (MPCs) have been successfully tested and evaluated in some studies [8, 9]. In addition, many other well-known linear control algorithms have been broadly tested on IPs by researchers to satisfy required control performances [10–12]. To address the substantial challenges regarding the communication between the controller and the plant, controllers with no bandwidth limitation in comparison with the ones using threshold-based communication have been investigated by Casanova et al. [13]. Also, Hamza et al. have provided a thorough real-time comparison of classical and state-of-the-art control techniques [14]. There also exist more complicated nonlinear controllers capable of global stabilization of IPs. These controllers employ gain scheduling, integral control, feedback linearization, Lyapunov redesign, backstepping, passively-based control, and high-gain observer to have a better performance. Many researchers have attempted to stabilize IPs with the variation and combination of the above-mentioned nonlinear controllers,

such as Interconnection and Damping Assignment Passively-Based Control (IDA-PBC) [15], cascade non-linear control [16–18], Sliding Mode Variable Structure Control (SMVSC) [19], hybrid control for global stabilization [20, 21], and nonlinear Model Predictive Controller (MPC) [22, 23], to name but a few [24–26]. However, having an analytical solution – a realtime, low-latency computation – of a closed-loop system offers a clear insight into how variables and control gains affect the result. In addition, the analytical solution can be employed as a reference system for the confirmation of numerical comes out. In this regard, quite a few methods have been proposed to find the analytical solution of nonlinear differential equations such as Hamilton approach [27], the parameter expansion method [28], homotropy perturbation method [29], and other well-known methods [30–32]. The exact analytical solution of nonlinear equation of a large amplitude simple open-loop system pendulum has been found by M. G. Sobamowo [33]. The dynamical response of an open-loop 3-DoF pendulum that is harmonically excited has been studied, and the analytical solution implementing the multiple scale method has been carried out [34]. Employing perturbative techniques, Ashrafiuon et al. [35] have presented an approximate analytical solution for the rotary inverted pendulum based on which the step response of the system using the sliding mode controller has been investigated. However, no investigation in the frequency domain has been done yet. In this paper, the analytical solution in the frequency domain has been calculated.

The dynamics of a nonlinear system is significantly richer than that of its linear counterparts, and there are several phenomena that can take place only in the presence of nonlinearity. Research have demonstrated that in the case of an IP the complexity would be even further increased if an elastic beam is used for suspension [36]. Arising from this inherent nonlinearity, the large amplitude vibration of IPs being linearly controlled and locally stabilized at the vicinity of their equilibrium position may lead to instabilities. The linearization of system equations in the neighborhood of the upright position of the pendulum within the design process of the linear controllers restricts their application to the cases with small amplitude disturbances and initial conditions. It necessitates adequate attention to be paid when the set point of the base position is continuously being changed in order to track a predefined path. That is because the existence of a frequency near the natural frequencies of the system in the actuation waveform may result in system instability through the occurrence of resonant large amplitude responses. As a result, although, linear experimental model analysis is broadly utilized in the complex structure of many types of inverted pendulums, leading to acceptable results, the substantial increase in computational power and the demand for higher performance of the inverted pendulum is encouraging researchers more than ever to take nonlinear effect into account and include nonlinearities in the design and analysis of complex engineering structures.

In the present study, the nonlinear vibratory response of a full-state feedback stabilized RIP, first introduced by Furuta et al. [37], is both analytically and experimentally investigated. To end this, first using Lagrange's equations the nonlinear coupled equations of the system incorporating the dynamics of the pendulum and the transfer function of the controller are derived. To verify the later obtained analytical results a rotary inverted pendulum is fabricated and its geometrical and inertial parameters together with the electrical parameters of the employed DC motor are measured accurately and introduced to the extracted equations. The nonlinear equations are then solved implementing the method of multiple scales for the case of forced oscillations. The primary resonant response of the system in the neighborhood of both natural frequencies is investigated, validated, and discussed. In addition, controller parameters are set in the process of deriving the solution and their effect on the frequency response of the system is studied.

2. Analytical Investigation

Figure 1 shows the schematic view of a rotary inverted pendulum using two rotary encoders as sensors and one DC motor as the actuator. The moving parts of the system may be divided into two groups where the parts at each group are fixed to each other and may be considered a single rigid body. The first group includes beam 1, rotating parts of encoder 1 (output shaft and the code disk), the rotor of the DC motor, the fixed parts of encoder 2 (the housing and electronics), and all coupling and connections used to connect them to each other. The second group is composed of the hanging beam (beam 2), the rotating parts of encoder 2, and the couplings used to connect them. Figure 2 clearly shows these two rigid bodies and the parts of the system from which they are composed. This figure includes a 3D model of the fabricated inverted pendulum used for experimental verification of the results which will be introduced in the next section. The total masses of the rigid bodies are represented by m_1, and m_2, respectively. In addition, r_1 and r_2 indicate the location of the center of gravity of mass m_2, where as shown in Fig. 1 the former denotes the distance of CG from the rotating axis of the motor and the latter is its distance from the rotating axis of encoder 2. To extract the governing dynamical equations of the system, Lagrange's method is adopted. According to this method, first the total kinetic and potential energies of the system should be determined. The velocity of the center of gravity of m_2 may be written as:

$$\vec{v}_2 = -\left(r_1\dot{\phi}\cos\theta + r_2\dot{\theta}\right)\hat{i} + \left(r_1\dot{\phi}\sin\theta\right)\hat{j} - \left(r_2\dot{\phi}\sin\theta\right)\hat{k} \quad (1)$$

The total angular velocity vector of the second rigid body written with respect to the coordinate system xyz, is:

$$\vec{\omega}_2 = -\left(\dot{\phi}\sin\theta\right)\hat{i} - \left(\dot{\phi}\cos\theta\right)\hat{j} + \left(\dot{\theta}\right)\hat{k}$$

2

Therefore, the total kinetic energy of the system will be:

$$T = \frac{1}{2}I_{\phi}\dot{\phi}^2 + \frac{1}{2}m_2\left[\left(r_1\dot{\phi}\cos\theta + r_2\dot{\theta}\right)^2 + \left({r_1}^2 + {r_2}^2\right)\left(\dot{\phi}\sin\theta\right)^2\right] + \frac{1}{2}I_{2x}\left(\dot{\phi}\sin\theta\right)^2 + \frac{1}{2}I_{2y}\left(\dot{\phi}\cos\theta\right)^2 + \frac{1}{2}I_{2z}\dot{\theta}^2 + I_{2yz}\dot{\phi}\dot{\theta}\cos\theta$$

3

where I_{φ} designates the the moment of inertia of m_1 about the motor axis. Also, I_{2x}, I_{2y}, I_{2z}, and I_{2yz} are the nonzero elements of the inertia tensor of m_2 about its mass center and with respect to a coordinate system connected to beam 2, as shown in Fig. 1.

The total potential energy of the system may be written as:

$$U = m_2 g r_2 \cos\theta$$

4

By definition, the Lagrangian of the system is:

$$L = T - U$$

5

Choosing φ and θ as our generalized coordinates, the Lagrange's equations of the system will be of the following form:

$$\frac{d}{dt}\left(\frac{\partial L}{\partial \dot{\alpha}}\right) - \frac{\partial L}{\partial \alpha} = Q_\alpha \qquad \alpha = \phi,\ \theta$$

6

The term Q_α in the above equation is the generalized nonconservative force and may be derived by calculation of the total virtual work done as:

$$\delta W_{nc} = Q_\phi \delta\phi + Q_\theta \delta\theta = \tau\delta\phi \quad \Rightarrow \quad Q_\phi = \tau, \quad Q_\theta = 0$$

7

where τ denotes the generated mechanical torque of the motor.

For a DC motor the torque applied to the rotor may be written as a function of its terminal voltage V and speed $\dot{\varphi}$ as:

$$\tau = \frac{1}{R_m}\left(\frac{V}{k_e} - \dot{\phi}\right)$$

8

where R_m and k_e are speed regulation and back EMF constants of the motor, respectively. It should be noted that the above equation neglects the inductance of the motor coil which according to the low frequencies involved in most mechanical systems is a reasonable assumption.

To make the pendulum stable at $\theta = 0$, a closed loop control scheme is used in this paper where the controller accepts φ, θ, $\dot{\varphi}$, and $\dot{\theta}$ as inputs and applies a voltage equal to $f_c(\varphi, \theta, \dot{\varphi}, \dot{\theta})$ to the motor. Considering this terminal voltage for the motor then substituting equations (1) to (5), (7), and (8) into (6), the governing equations of the system are derived as:

$$\begin{cases} \left(I_1 + I_2\sin^2\theta\right)\ddot{\phi} + \left(I_3\cos\theta\right)\ddot{\theta} + \left(I_2\sin 2\theta\right)\dot{\phi}\dot{\theta} - \left(I_3\sin\theta\right)\dot{\theta}^2 + \dfrac{1}{R_m}\dot{\phi} = \dfrac{f_c\left(\phi,\ \theta,\ \dot{\phi},\ \dot{\theta}\right)}{R_m k_e} \\ \left(I_3\cos\theta\right)\ddot{\phi} + I_4\ddot{\theta} - \dfrac{1}{2}\left(I_2\sin 2\theta\right)\dot{\phi}^2 - m_2 g r_2 \sin\theta = 0 \end{cases}$$

9

where:

$$I_1 = I_\phi + I_{2y} + m_2 {r_1}^2,\ I_2 = I_{2x} - I_{2y} + m_2 {r_2}^2,\ I_3 = I_{2yz} + m_2 r_1 r_2,\ I_4 = I_{2z} + m_2 {r_2}^2$$

10

The equilibrium points of the system may be found by replacing all terms containing time derivatives of the variable by zero which results in:

$$\begin{cases} f_c(\phi,\ \theta,\ 0,\ 0) = 0 & (a) \\ \sin\theta = 0 & (b) \end{cases}$$

11

Therefore, $\theta = 0$ and $\varphi = \varphi_d$ is an equilibrium point of the system if and only if $f_c\left(\varphi_d, 0, 0, 0\right) = 0$. As a consequence, assuming the function f_c to be linear, it may be written as:

$$f_c\left(\phi,\ \theta,\ \dot{\phi},\ \dot{\theta}\right) = k_1\left(\phi - \phi_d\right) + k_2\theta + k_3\dot{\phi} + k_4\dot{\theta}$$

12

It should be noted that in practice there may be an error or an offset in θ measurement and, hence, the point at which the measured θ vanishes may not exactly coincide with the angle at which CG is accurately located above the axis of the second encoder. Therefore, Eq. (11-a) will not hold anymore, and consequently $\theta = 0$ will not be an equilibrium point for the closed-loop system. To overcome this problem even if the position angle of the first beam i.e., φ is not intended to be controlled at any desired position φ_d the term $k_1\varphi$ must exist in f_c. By creating a small error between the angle φ and its desired value φ_d (or with 0 when φ_d is not important), this term makes Eq. (11-a) hold. Additionally, by employing this term the system will be able to suspend the pendulum stably at any arbitrary given φ_d.

Substituting Eq. (12) into (9) while replacing $\sin\theta$ and $\cos\theta$ by their Taylor's series around $\theta = 0$ and keeping the nonlinear terms up to third order results in:

$$\begin{cases} I_1\ddot{\phi} + I_3\ddot{\theta} + \dfrac{1}{R_m}\dot{\phi} - \dfrac{k_2}{R_m k_e}\theta - \dfrac{k_1}{R_m k_e}\phi = -\dfrac{k_1}{R_m k_e}\phi_d + I_2\left(\dfrac{4}{3}\dot{\theta}\dot{\phi}\theta^3\right) + I_3\left(\dfrac{1}{2}\ddot{\theta}\theta^2 + \dot{\theta}^2\theta - \dfrac{1}{3}\dot{\theta}^2\theta^3\right) \\ \qquad - I_2\left(\ddot{\phi}\theta^2 + 2\dot{\theta}\dot{\phi}\theta\right) + \dfrac{1}{R_m}\left(\dfrac{k_3}{k_e} - 1\right)\dot{\phi} + \dfrac{k_4\dot{\theta}}{R_m k_e} \\ I_3\ddot{\phi} + I_4\ddot{\theta} - m_2 g r_2\theta = \dfrac{1}{2}I_2\left(2\theta\dot{\phi}^2 - \dfrac{4}{3}\theta^3\dot{\phi}^2\right) + \dfrac{1}{2}I_3\ddot{\varphi}\theta^2 - \dfrac{1}{6}m_2 g r_2\theta^3 \end{cases}$$

13

The above set of nonlinear equations may be analytically solved employing the perturbation method of multiple scales. To do this, first of all by assuming the amplitude of angular displacements of φ and θ to be of order of a small parameter denoted by ϵ, one can write:

\phi =\varepsilon {\phi _1}+{\varepsilon ^3}{\phi _3},\,\,\,\,\,\,\,\,\,\,\,\,\,\,\theta =\varepsilon {\theta _1}+{\varepsilon ^3}{\theta _3}

14

Furthermore, assuming the damping and excitation terms to be of order of {ϵ}^{3}, one can let:

{\phi _d}={\varepsilon ^3}{\Phi _d},\,\,\,\,\,\,\,\,\,\,\,\,\,\,\,\,\,\,\frac{{{k_3}}}{{{k_e}}} - 1={\varepsilon ^2}{K_3},\frac{{{k_4}}}{{{k_e}}}={\varepsilon ^2}{K_4}

15

New independent variables called time scales may be introduced accordingly as:

{T_0}=t,\,\,\,\,\,\,\,\,\,{T_2}={\varepsilon ^2}t

16

Representing the operator denoting partial differentiation with respect to {T}_{n} by {D}_{n} (i.e., {D}_{n}=\frac{\partial }{\partial {T}_{n}}) and using the chain rule of differentiation, one can write operators denoting first and second derivatives with respect to t as an expansion of {D}_{n}s and their multiplications as:

\frac{d}{{dt}}={D_0}+{\varepsilon ^2}{D_2},\frac{{{d^2}}}{{d{t^2}}}=D_{0}^{2}+2{\varepsilon ^2}{D_0}{D_2}

17

Substituting equations (14), (15), and (17) into (13), then separating terms of different orders of ϵ, one has:

{\varepsilon ^1}:\left\{ \begin{gathered} {I_1}D_{0}^{2}{\phi _1}+{I_3}D_{0}^{2}{\theta _1} - \frac{{{k_1}}}{{{R_m}{k_e}}}{\phi _1} - \frac{{{k_2}}}{{{R_m}{k_e}}}{\theta _1}=0\, \hfill \\ {I_3}D_{0}^{2}{\phi _1}+{I_4}D_{0}^{2}{\theta _1} - {m_2}g{r_2}{\theta _1}=0 \hfill \\ \end{gathered} \right.

18

{\varepsilon ^3}:\left\{ \begin{gathered} {I_1}D_{0}^{2}{\phi _3}+{I_3}D_{0}^{2}{\theta _3} - \frac{{{k_2}}}{{{R_m}{k_e}}}{\theta _3} - \frac{{{k_1}}}{{{R_m}{k_e}}}{\phi _3}={f_1} \hfill \\ {I_3}D_{0}^{2}{\phi _3}+{I_4}D_{0}^{2}{\theta _3} - {m_2}g{r_2}{\theta _3}={f_2} \hfill \\ \end{gathered} \right.

19

where:

\begin{gathered} {f_1}= - 2{I_1}{D_0}{D_2}{\phi _1} - 2{I_3}{D_0}{D_2}{\theta _1} - \frac{{{k_1}}}{{{R_m}{k_e}}}{\Phi _d}\,+{I_2}\left({2{D_0}{\theta _1}{D_0}{\phi _1}{\theta _1}+{\theta _1}^{2}D_{0}^{2}{\phi _1}} \right) \hfill \\ \,\,\,\,\,\,\,\,\,\,\,\,{\text{ }}+{I_3}\left[{{{\left({{D_0}{\theta _1}} \right)}^2}{\theta _1}+\frac{1}{2}D_{0}^{2}{\theta _1}{\theta _1}^{2}} \right]+\frac{{{K_3}}}{{{R_m}}}{D_0}{\phi _1}+\frac{{{K_4}}}{{{R_m}}}{D_0}{\theta _1} \hfill \\ {f_2}= - 2{I_3}{D_0}{D_2}{\phi _1} - 2{I_4}{D_0}{D_2}{\theta _1}+{I_2}{\left({{D_0}{\phi _1}} \right)^2}{\theta _1}+\frac{1}{2}{I_3}D_{0}^{2}{\phi _1}{\theta _1}^{2} - \frac{1}{6}{m_2}g{r_2}{\theta _1}^{3} \hfill \\ \end{gathered}

20

The general solution of Eq. (18) may be written as:

\begin{gathered} {\phi _1}={A_1}\exp \left({i{\omega _1}{T_0}} \right)+{A_2}\exp \left({i{\omega _2}{T_0}} \right)+cc \hfill \\ {\theta _1}={\alpha _1}{A_1}\exp \left({i{\omega _1}{T_0}} \right)+{\alpha _2}{A_2}\exp \left({i{\omega _2}{T_0}} \right)+cc \hfill \\ \end{gathered}

21

where cc denotes the complex conjugate terms. The above solution assumes that the following equation from which {\omega }_{1} and {\omega }_{2} may be calculated, has four real roots:

$$\left({{I_1}{I_4} - {I_3}^{2}} \right){\omega ^4}+\left[{\frac{1}{{{R_m}{k_e}}}\left({{k_1}{I_4} - {k_2}{I_3}} \right)+{I_1}{m_2}g{r_2}} \right]{\omega ^2}+\frac{{{k_1}}}{{{R_m}{k_e}}}{m_2}g{r_2}=0$$
22
This condition needs ${k}_{1}$ and ${k}_{2}$ to be chosen so that the following inequalities hold:

$$\begin{gathered} {k_1}>0 \hfill \\ {k_2}>\frac{{{k_1}{I_4}+{R_m}{k_e}{I_1}{m_2}g{r_2}}}{{{I_3}}} \hfill \\ {\left[{\frac{1}{{{R_m}{k_e}}}\left({{k_1}{I_4} - {k_2}{I_3}} \right)+{I_1}{m_2}g{r_2}} \right]^2}>\frac{{4{k_1}}}{{{R_m}{k_e}}}{m_2}g{r_2}\left({{I_1}{I_4} - {I_3}^{2}} \right) \hfill \\ \end{gathered}$$
23
The coefficients ${\alpha }_{1}$ and ${\alpha }_{2}$ in Eq. (21) are as follows:

$${\alpha _i}= - \frac{{{I_3}{\omega _i}^{2}}}{{\left({{m_2}g{r_2}+{I_4}{\omega _i}^{2}} \right)}}\,\,\,\,\,\,\,\,\,i=1,2$$
24
To analyze resonance occurrence in the neighborhood of the natural frequencies of the system, one may let:

$${\Phi _d}={E_1}\cos \left({{\Omega _1}t} \right)+{E_2}\cos \left({{\Omega _2}t} \right)$$
25
where ${\varOmega }_{1}$ and ${\varOmega }_{2}$ differ ${\omega }_{1}$ and ${\omega }_{2}$ by small parameters ${\sigma }_{1}$ and ${\sigma }_{2}$, respectively, as:

$$\begin{gathered} {\Omega _1}={\omega _1}+{\varepsilon ^2}{\sigma _1} \hfill \\ {\Omega _2}={\omega _2}+{\varepsilon ^2}{\sigma _2} \hfill \\ \end{gathered}$$
26
To eliminate the secular terms in Eq. (18), the coefficients of the terms $\text{e}\text{x}\text{p}\left(i{\omega }_{i}{T}_{0}\right)$ in the following expressions must vanish:

$${\beta _i}{f_1}+{f_2}$$
27
where:

$${\beta _i}= - \frac{{{I_3}\omega _{i}^{2}}}{{\left({{I_1}\omega _{i}^{2}+\frac{{{k_1}}}{{{R_m}{k_e}}}} \right)}}\,\,\,\,\,\,\,\,\,i=1,2$$
28
Substituting equations (21), (25), and (26) into (27), one obtains:

$$\left\{ \begin{gathered} i{c_{11}}{D_2}{A_1}+\frac{{{\beta _1}{k_1}}}{{2{R_m}{k_e}}}{E_1}\exp \left({i{\sigma _1}{T_2}} \right) - \frac{{{\beta _1}}}{{{R_m}}}({K_3}+{K_4}{\alpha _1}){A_1}i{\omega _1}+{c_{21}}{A_1}^{2}{{\bar {A}}_1}+{c_{31}}{A_1}{A_2}{{\bar {A}}_2}=0 \hfill \\ i{c_{12}}{D_2}{A_2}+\frac{{{\beta _2}{k_1}}}{{2{R_m}{k_e}}}{E_2}\exp \left({i{\sigma _2}{T_2}} \right) - \frac{{{\beta _2}}}{{{R_m}}}({K_3}+{K_4}{\alpha _3}){A_2}i{\omega _2}+{c_{32}}{A_1}{{\bar {A}}_1}{A_2}+{c_{22}}{A_2}^{2}{{\bar {A}}_2}=0 \hfill \\ \end{gathered} \right.$$
29
where:

$$\begin{gathered} {c_{11}}=2{\omega _1}\left[{{\beta _1}{I_1}+{I_3}\left({1+{\alpha _1}{\beta _1}} \right)+{I_4}{\alpha _1}} \right] \hfill \\ {c_{21}}={\alpha _1}\left\{ {\left[{{I_2}\left({1+{\beta _1}{\alpha _1}} \right)+\frac{1}{}\right.}\right.$$

{2}{l_3}{\alpha _1}\left({3+{\beta _1}{\alpha _1}} \right)} \right]{\omega _1}^{2}+\frac{1}{2}{m_2}g{r_2}{\alpha _1}^{2}} \right\} \hfill \\ {c_{31}}=\left[{{\beta _1}\left({2{l_2}+{l_3}{\alpha _1}} \right)+{l_3}} \right]{\alpha _2}^{2}{\omega _1}^{2}+2\left({{l_2}+{l_3}{\alpha _2}} \right){\alpha _1}{\omega _2}^{2}+{m_2}g{r_2}{\alpha _1}{\alpha _2}^{2} \hfill \\ {c_{12}}=2{\omega _2}\left[{{\beta _2}{l_1}+{l_3}\left({1+{\alpha _2}{\beta _2}} \right)+{l_4}{\alpha _2}} \right] \hfill \\ {c_{22}}={\alpha _2}\left\{ {\left[{{l_2}\left({1+{\beta _2}{\alpha _2}} \right)+\frac{1}{2}{l_3}{\alpha _2}\left({3+{\beta _2}{\alpha _2}} \right)} \right]{\omega _2}^{2}+\frac{1}{2}{m_2}g{r_2}{\alpha _2}^{2}} \right\} \hfill \\ {c_{32}}=\left[{{\beta _2}\left({2{l_2}+{l_3}{\alpha _2}} \right)+{l_3}} \right]{\alpha _1}^{2}{\omega _2}^{2}+2\left({{l_2}+{l_3}{\alpha _1}} \right){\alpha _2}{\omega _1}^{2}+{m_2}g{r_2}{\alpha _2}{\alpha _1}^{2} \hfill \\ \end{gathered}

30

Eliminating the excitation and nonlinear terms from the above expressions, the condition for linear stability of the system is derived as:

\frac{{{\beta _1}\left({{K_3}+{K_4}{\alpha _1}} \right){\omega _1}}}{{{R_m}{c_{11}}}}cript>

31

Amplitudes {A}_{1} and {A}_{2} may be represented by polar form as:

{A_1}=\frac{1}{2}{a_1}{e^{i{\psi _1}}},\,\,\,\,\,\,\,\,\,\,\,\,\,\,\,\,{A_2}=\frac{1}{2}{a_2}{e^{i{\psi _2}}}

32

Substituting the above equation into Eq. (29) one has:

\left\{ \begin{gathered} \frac{{i{c_{11}}}}{2}\left({{a_1}^{\prime }+i{\psi _1}^{\prime }{a_1}} \right)+\frac{{{\beta _1}{k_1}}}{{2{R_m}{k_e}}}{E_1}\exp \left({i{\sigma _1}{T_2} - i{\psi _1}} \right) - \frac{{{\beta _1}}}{{2{R_m}}}\left({{K_3}+{K_4}{\alpha _1}} \right)i{\omega _1}{a_1}+\frac{1}{8}{c_{21}}{a_1}^{3}+\frac{1}{8}{c_{31}}{a_1}{a_2}^{2}=0 \hfill \\ \frac{{i{c_{12}}}}{2}\left({{a_2}^{\prime }+{a_2}i{\psi _2}^{\prime }} \right)+\frac{{{\beta _2}{k_1}}}{{2{R_m}{k_e}}}{E_2}\exp \left({i{\sigma _2}{T_2} - i{\psi _2}} \right) - \frac{{{\beta _2}}}{{2{R_m}}}\left({{K_3}+{K_4}{\alpha _2}} \right)i{\omega _2}{a_2}+\frac{1}{8}{c_{22}}{a_2}^{3}+\frac{1}{8}{c_{32}}{a_1}^{2}{a_2}=0 \hfill \\ \end{gathered} \right.

33

By the separation of real and imaginary parts in Eq. (33) and introduction of the following new variables:

\begin{gathered} {\gamma _1}={\sigma _1}{T_2} - {\psi _1} \hfill \\ {\gamma _2}={\sigma _2}{T_2} - {\psi _2} \hfill \\ \end{gathered}

34

the following set of autonomous equations are found:

\left\{ \begin{gathered} {c_{11}}{a_1}^{\prime }=\frac{{{\beta _1}}}{{{R_m}}}\left({{K_3}+{K_4}{\alpha _1}} \right){\omega _1}{a_1} - \frac{{{\beta _1}{k_1}}}{{2{R_m}{k_e}}}{E_1}\sin {\gamma _1} \hfill \\ {c_{11}}{a_1}{\gamma _1}^{\prime }={c_{11}}{a_1}{\sigma _1} - \frac{1}{4}{c_{21}}{a_1}^{3} - \frac{1}{4}{c_{31}}{a_1}{a_2}^{2} - \frac{{{\beta _1}{k_1}}}{{2{R_m}{k_e}}}{E_1}\cos {\gamma _1} \hfill \\ {c_{12}}{a_2}^{\prime }=\frac{{{\beta _2}}}{{{R_m}}}\left({{K_3}+{K_4}{\alpha _2}} \right){\omega _2}{a_2} - \frac{{{\beta _2}{k_1}}}{{2{R_m}{k_e}}}{E_2}\sin {\gamma _2} \hfill \\ {c_{12}}{a_2}{\gamma _2}^{\prime }={c_{12}}{a_2}{\sigma _2} - \frac{1}{4}{c_{22}}{a_2}^{3} - \frac{1}{4}{c_{32}}{a_1}^{2}{a_2} - \frac{{{\beta _2}{k_1}}}{{2{R_m}{k_e}}}{E_2}\cos {\gamma _2} \hfill \\ \end{gathered} \right.

35
The equilibrium points of the above dynamical system may be found by substituting {a}_{1}^{\text{'}}= {a}_{2}^{\text{'}}={\gamma }_{1}^{\text{'}}={\gamma }_{2}^{\text{'}}=0, leading to the following set of equations for {a}_{1} and {a}_{2}:

\left\{ \begin{gathered} {\left[{\frac{{{\beta _1}}}{{2{R_m}}}({K_3}+{K_4}{\alpha _1}){\omega _1}{a_1}} \right]^2}+ {\left({\frac{1}{2}{c_{11}}{a_1}{\sigma _1} - \frac{1}{8}{c_{21}}{a_1}^{3} - \frac{1}{8}{c_{31}}{a_1}{a_2}^{2}} \right)^2}={\left({\frac{{{\beta _1}{k_1}}}{{2{R_m}{k_e}}}{E_1}} \right)^2} \hfill \\ {\left[{\frac{{{\beta _2}}} {{2{R_m}}}({K_3}+{K_4}{\alpha _2}){\omega _2}{a_2}} \right]^2}+{\left({\frac{1}{2}{c_{12}}{a_2}{\sigma _2} - \frac{1}{8}{c_{22}}{a_2}^{3} - \frac{1}{8}{c_{32}}{a_1}^{2}{a_2}} \right)^2}={\left({\frac{{{\beta _2}{k_1}}}{{2{R_m} {k_e}}}{E_2}} \right)^2} \hfill \\ \end{gathered} \right.
36
The above equation may be solved to calculate vibration amplitudes {a}_{1} and {a}_{2} as functions of the excitations amplitude {E}_{1}, {E}_{2} and deviations {\sigma }_{1} and {\sigma }_{2} from the natural frequencies of the system. That is while to depict the response curves, it suffices to simply calculate {\sigma }_{1}, {\sigma }_{2}, {E}_{1}, and {E}_{2} by a rearrangement of Eq. (36) as:

\begin{gathered} {\sigma _1}=\frac{{\frac{1}{4}{c_{21}}{a_1}^{3}+\frac{1}{4}{c_{31}}{a_1}{a_2}^{2} \pm \sqrt {{{\left({\frac{{{\beta _1}{k_1}}}{{2{R_m}{k_e}}}{E_1}} \right)}^2} - {{\left[{\frac{{{\beta _1}}}{{2{R_m}}}({K_3}+{K_4} {\alpha _1}){\omega _1}{a_1}} \right]}^2}} }}{{c_{11}}{a_1}}} \hfill \\ {\sigma _2}=\frac{{\frac{1}{4}{c_{22}} {a_2}^{3}+\frac{1}{4}{c_{32}}{a_1}^{2}{a_2} \pm \sqrt {{{\left({\frac{{{\beta _2}{k_1}}}{{2{R_m}{k_e}}}{E_2}} \right)}^2} - {{\left[{\frac{{{\beta _2}}}{{2{R_m}}}({K_3}+{K_4}{\alpha _2}){\omega _2}{a_2}} \right]}^2}} }}{{c_{12}} {a_2}}} \hfill \\ {E_1}=\frac{{{R_m}{k_e}}}{{{\beta _1}{k_1}}}\sqrt {{{\left[{\frac{{{\beta _1}}}{{{R_m}}}({K_3}+{K_4} {\alpha _1}){\omega _1}{a_1}} \right]}^2}+{{\left({{c_{11}}{a_1}{\sigma _1} - \frac{1}{4}{c_{21}}{a_1}^{3} - \frac{1} {4}{c_{31}}{a_1}{a_2}^{2}} \right)}^2}} \hfill \\ {E_2}=\frac{{{R_m}{k_e}}}{{{\beta _2}{k_1}}}\sqrt {{{\left[{\frac{{{\beta _2}}}{{{R_m}}}({K_3}+{K_4}{\alpha _2}){\omega _2}{a_2}} \right]}^2}+{{\left({{c_{12}}{a_2}{\sigma _2} - \frac{1}{4} {c_{22}}{a_2}^{3} - \frac{1}{4}{c_{32}}{a_1}^{2}{a_2}} \right)}^2}} \hfill \\ \end{gathered}
37
To explore how the inherent geometric nonlinearity of the pendulum affects the behavior of the system, a linear solution to the governing equations is performed as well. The results of the linear solution are used along with the results of the nonlinear solution when comparing the analytical, numerical, and experimental findings in the next section. The first step toward this linear solution is eliminating the nonlinear terms in Eq. (13) which results in:

\left\{ \begin{gathered} {I_1}\ddot {\phi }+{I_3}\ddot {\theta } - \frac{{{k_2}}}{{{R_m}{k_e}}}\theta - \frac{{{k_1}}} {{{R_m}{k_e}}}\phi = - \frac{{{k_1}}}{{{R_m}{k_e}}}{\phi _d}+\frac{1}{{{R_m}}}\left({\frac{{{k_3}}}{{{k_e}}} - 1} \right)\dot {\phi }+\frac{{{k_4}\dot {\theta }}}{{{R_m}{k_e}}} \hfill \\ {I_3}\ddot {\phi }+{I_4}\ddot {\theta } - {m_2}g{r_2}\theta =0 \hfill \\ \end{gathered} \right.
38
where {\varphi }_{d} is a single harmonic excitation as:

{\phi _d}=E\exp \left({i\omega t} \right)
39

Substituting the above expression into Eq. (37), the steady state solutions for \varphi and \theta are found to be of the following form:

$$\begin{gathered} \phi =\Phi \exp \left({i\omega t} \right) \hfill \\ \theta =\Theta \exp \left({i\omega t} \right) \hfill \\ \end{gathered}$$
40
where {\Phi } and {\Theta } are complex amplitudes, derived from the following equation:

$$\left\{ \begin{gathered} \left[{{I_1}{\omega ^2}+\frac{{{k_1}}}{{{R_m}{k_e}}}+\frac{1}{{{R_m}}}\left({\frac{{{k_3}}}{{{k_e}}} - 1} \right)j\omega } \right]\Phi +\left({{I_3}{\omega ^2}+\frac{{{k_2}}}{{{R_m}{k_e}}}+\frac{{{k_4}}}{{{R_m}{k_e}}}j\omega } \right)\Theta =\frac{{{k_1}}}{{{R_m}{k_e}}}{E_1} \hfill \\ {I_3}{\omega ^2}\Phi +\left({{I_4}{\omega ^2}+{m_2}g{r_2}} \right)\Theta =0 \hfill \\ \end{gathered} \right.$$
41
Solving the above equation, one obtains:

$$\left\{ \begin{gathered} \Phi =\frac{{\left({{I_4}{\omega ^2}+{m_2}g{r_2}} \right){k_1}{E_1}}}{{{R_m}{k_e}\left\{ {\left({{I_4}{\omega ^2}+{m_2}g{r_2}} \right)\left[{{I_1}{\omega ^2}+\frac{{{k_1}}}{{{R_m}{k_e}}}+\frac{1}{{{R_m}}}\left({\frac{{{k_3}}}{{{k_e}}} - 1} \right)j\omega } \right] - \left({{I_3}{\omega ^2}+\frac{{{k_2}}}{{{R_m}{k_e}}}+\frac{{{k_4}}}{{{R_m}{k_e}}}j\omega } \right){I_3}{\omega ^2}} \right\}} \hfill \\ \Theta = - \frac{{{I_3}{\omega ^2}{k_1}{E_1}}}{{{R_m}{k_e}\left\{ {\left({{I_4}{\omega ^2}+{m_2}g{r_2}} \right)\left[{{I_1}{\omega ^2}+\frac{{{k_1}}}{{{R_m}{k_e}}}+\frac{1}{{{R_m}}}\left({\frac{{{k_3}}}{{{k_e}}} - 1} \right)j\omega } \right] - \left({{I_3}{\omega ^2}+\frac{{{k_2}}}{{{R_m}{k_e}}}+\frac{{{k_4}}}{{{R_m}{k_e}}}j\omega } \right){I_3}{\omega ^2}} \right\}} \hfill \\ \end{gathered} \right.$$
42

3. Experimental Setup

A photo of the fabricated rotary inverted pendulum with the aim of being used to verify the analytical results is shown in Fig. 3. The measured and calculated values for the parameters of the system are as given in Table 1. The electric parameters of the motor are determined by measuring the input current in both no-load and locked-rotor conditions. To obtain an accurate estimation of the structural parameters of the system, they are calculated using Solidworks software. To end this, first a precise 3D model of the system is generated with corresponding materials assigned to all the parts and then the total mass, moment of inertia and the location of center of mass is calculated for the parts forming rigid bodies 1 and 2 (See Fig. 2). All the analytical and numerical results presented in the next section are for a system with parameters as given in Table 1.

Table 1
Measured parameters of the system

	Description	Symbol	Value
Structure parameters	Moment of inertia of part 1 about the motor axis	{I}_{\varphi}	2.31\times {10}^{-4} kg.{m}^{2}
	Mass of part 2	{m}_{2}	0.088 kg
	Moment of inertia of part 2 about x-axis	{I}_{2x}	2.81\times {10}^{-4} kg.{m}^{2}
	Moment of inertia of part 2 about y-axis	{I}_{2y}	9.67\times {10}^{-6} kg.{m}^{2}
	Moment of inertia of part 2 about z-axis	{I}_{2z}	2.89\times {10}^{-4} kg.{m}^{2}
	Product of inertia about yz-plane	{I}_{yz}	3.07\times {10}^{-5} kg.{m}^{2}
	Distance from the center of gravity of part 2 to the motor axis	{r}_{1}	13.40 cm
	Distance from the center of gravity of part 2 to encoder 2 axis	{r}_{2}	5.80 cm
Motor parameters	Back EMF constant	{k}_{e}	4.88\times {10}^{-2} V.s/rad
	Speed regulation constant	{R}_{m}	2103 rad/N.m.s

4. Results Verification And Discussion

In this section, we present and compare the analytical, numerical, and experimental results. At first, the acceptable values of {k}_{1} and {k}_{2} for which the system is stable are determined based on inequalities of Eq. (23). By depicting the corresponding curves, one may find the acceptable area illustrated in Fig. 4. {k}_{1} and {k}_{2} can also be found either experimentally or through any other methods of control such as pole-placement or LQR. After finding an appropriate set of values for {k}_{1} and {k}_{2} to be 50 and 250, respectively, natural frequencies of the present 2-DoF system can be calculated by substituting the obtained values of {k}_{1} and {k}_{2} along with the measured parameters listed in Table 1 into Eq. (22). By doing so, the natural frequencies of the system are found to be {\omega }_{1}=4.24 \text{r}\text{a}\text{d}/\text{s}\text{e}\text{c} and {\omega }_{2}=50.2 \text{r}\text{a}\text{d}/\text{s}\text{e}\text{c}. Figure 5 illustrates the acceptable area for {k}_{3} and {k}_{4} found by depicting the inequalities of Eq. (31). Acceptable values of these state feedback gain lead to an asymptotically stable system.

Figure 6 through Fig. 9 show the analytically-calculated frequency responses of the system including both angular displacements \theta and \varphi in the neighborhood of the first and second resonances for different amplitudes of excitation. To verify the performed analytical solution, the governing equations are also numerically solved employing the Runge-Kutta method. The results of this numerical solution are depicted together with the analytical resonance curves in Fig. 6 to Fig. 9 for the comparison purposes where a very good agreement is observed. As these figures demonstrate, at small amplitudes of excitation the resonance curves are

almost symmetric resembling the behavior of a linear oscillator. This occurs while as excitation amplitude increases this symmetry gradually disappears through bending of the curves. As evidenced by the results, the nonlinearity has a hardening effect on the response curve in the neighborhood of the first resonance, while at the second resonance the system shows a softening behavior and the curve is bended toward lower frequencies. Another important point which can be inferred from Fig. 6 to Fig. 9 is the different levels of agreement between analytical and numerical results in different frequency bands. Although these two solutions are in a good agreement in the vicinity of the resonance peak, they start to diverge as the excitation frequency moves away from the natural one. This occurs because the perturbation solution assumes the detuning parameter \sigma to be of order {\epsilon}^{2} (See Eq. (26)) and therefore is valid only in a close neighborhood of the natural frequency.

One of the significant characteristics of these nonlinear frequency responses is the existence of a multivalued region which emerges and widens as the excitation amplitude increases. In this region, the curve is composed of three branches including one middle branch with saddle stability enveloped by two low and high energy stable branches. There are two bifurcation points of the saddle-node type in which a saddle point and a stable node of the system collides and annihilate each other. The location of these bifurcation points indicates the edges of the multivlued interval and the trajectory of the excitation (trajectory of {\varphi }_{d} in this case) determines whether the response falls on the upper branch of the curve or the lower one in this region. Figure 10 clearly demonstrates the evolution of a fully nonlinear response curve from an almost symmetric linear-like one as the excitation amplitude continuously grows.

To demonstrate the interaction of vibration modes corresponding to different natural frequencies, vibration amplitudes are depicted as surfaces that are functions of both {\sigma }_{1} and {\sigma }_{2} in Fig. 11 and Fig. 12. As these figures illustrate, while {a}_{2} is affected by frequencies of both excitation terms (See Eq. (25)), the variation of {a}_{1} as the frequency of second mode excitation changes is negligible. The effect of excitation amplitudes on the amplitude of the response at both modes of vibration is shown in Fig. 13 and Fig. 14. Additionally, Fig. 15 through Fig. 18 show the amplitude of the response for both \theta and \varphi with respect to the amplitude of excitations for several values of {\sigma }_{1} and {\sigma }_{2} which, as expected, contain both multivaluedness and jump phenomenon, resulting from the nonlinear phase-amplitude interaction governed by Eq. (35).

To verify our analytical and numerical solutions, the frequency response curves of the system for both \theta and \varphi at the first resonance are found through experimental measurements as well. The results are provided in Fig. 19 and Fig. 20 together with the numerical and analytical solutions. It is worth noting that the experiments are conducted at constant amplitude of excitation, while the angular frequency is increasing with the step size of 0.2 \text{r}\text{a}\text{d}/\text{s}\text{e}\text{c}. The analytical linear solution as derived in Eq. (42) is depicted together with the nonlinear response in these figures to demonstrate how the experimental results deviate from the symmetric curve resulting from the performed linear analysis. As can be clearly seen, in the close neighborhood of the natural frequency the linear solution leads to a considerable error, while the nonlinear one resembles the experimental behavior to a large extent.

5. Conclusion

In this paper, the nonlinear vibration behavior of a linearly controlled rotary inverted pendulum (RIP) is investigated through analytical simulations and experimental measurements. The perturbation method of

multiple scales is employed to solve the governing coupled nonlinear equations of the system derived through the implementation of the Lagrange's variational principle. The obtained analytical solution for the 2-DoF dynamical system in the frequency domain provides a clear-cut understanding of the behavior of the system the is subjected to the excitation force. To experimentally verify the predicted results of the analytical model, both of its mechanical and electrical parameters are set to be equal to those of the real RIP system employed in the experiment. The comparison of the results obtained through the analytical, numerical, and experimental approaches reveals a good agreement among them. The acceptable range of values for the controller feedback gains, leading to the stabilized oscillatory motion of the pendulum, is derived through the performed analyses. The findings indicate that, while the nonlinearity involved in the first mode of the vibration is a hardening type, the system shows a softening behavior when excited in the vicinity of its second natural frequency. As the amplitude of the alternating part of the desired position waveform is enhanced due to the bending of the resonance curves, large oscillations are possible to occur within a wider frequency band around the natural frequencies. This calculated frequency band must be avoided in practice when the set-point of the system is being changed as time passes, particularly in the case of periodic motions.

6. Declarations

Funding No funding was received to assist with the preparation of this manuscript.

Financial interests The authors declare they have no financial interests.

Compliance with ethical standards

Conflicts of interest The authors declare that they have no conflict of interest.

Availability of data and material The authors confirm that all data underlying the findings are fully available without restriction.

Authors' Contribution All authors contributed to the study conception and design. Material preparation, data collection and analysis were performed by Mohammadjavad Rahimi Dolatabad and Abdolreza Pasharavesh. The first draft of the manuscript was written by Mohammadjavad Rahimi Dolatabad and all authors commented on previous versions of the manuscript. Dr. A. Khayyat and Dr. A. Pasharavesh read and approved the final manuscript.

References

1. Aguilar-Avelar, C., Moreno-Valenzuela, J.: A composite controller for trajectory tracking applied to the Furuta pendulum. ISA Trans. **57**, 286–294 (2015)
2. Fang, Y., et al.: Nonlinear coupling control laws for an underactuated overhead crane system. IEEE/ASME transactions on mechatronics **8**(3), 418–423 (2003)
3. Chen, Y.-F., Huang, A.-C.: Controller design for a class of underactuated mechanical systems. IET control theory & applications **6**(1), 103–110 (2012)
4. Babu, J., Varghese, E.: *Stabilization of Rotary Arm Inverted Pendulum using State Feedback Techniques.* International Journal of Engineering Research & Technology (IJERT) ISSN: p. 2278 – 0181

5. Furuta, K., Okutani, T., Sone, H.: Computer control of a double inverted pendulum. Comput. Electr. Eng. **5**(1), 67–84 (1978)
6. Morasso, P., et al.: Stabilization of a cart inverted pendulum: improving the intermittent feedback strategy to match the limits of human performance. Front. Comput. Neurosci. **13**, 16 (2019)
7. Bettayeb, M., et al.: Stabilization of an inverted pendulum-cart system by fractional PI-state feedback. ISA Trans. **53**(2), 508–516 (2014)
8. Jezierski, A., Mozaryn, J., Suski, D.. *A comparison of LQR and MPC control algorithms of an inverted pendulum*. in *Polish Control Conference*. 2017. Springer
9. Prasad, L.B., Tyagi, B., Gupta, H.O.: Optimal control of nonlinear inverted pendulum system using PID controller and LQR: performance analysis without and with disturbance input. Int. J. Autom. Comput. **11**(6), 661–670 (2014)
10. Jain, A., Tayal, D., Sehgal, N.: *Control of non-linear inverted pendulum using fuzzy logic controller*. International Journal of Computer Applications, 2013. 69(27)
11. Hassanzadeh, I., Mobayen, S., *Controller design for rotary inverted pendulum system using evolutionary algorithms.* Mathematical Problems in Engineering, 2011. **2011**
12. Olfati-Saber, R.. *Fixed point controllers and stabilization of the cart-pole system and the rotating pendulum*. in *Proceedings of the 38th IEEE Conference on Decision and Control (Cat. No. 99CH36304)*. 1999. IEEE
13. Casanova, V., et al.: Control of the rotary inverted pendulum through threshold-based communication. ISA Trans. **62**, 357–366 (2016)
14. Hamza, M., et al.: Real-time control of an inverted pendulum: A comparative study. In: 2011 Frontiers of Information Technology. IEEE (2011)
15. Yokoyama, K., Takahashi, M.: Stabilization of a cart-inverted pendulum with interconnection and damping assignment passivity-based control focusing on the kinetic energy shaping. Journal of System Design and Dynamics **4**(5), 698–711 (2010)
16. Zhang, C., et al.: Cascaded control for balancing an inverted pendulum on a flying quadrotor. Robotica **35**(6), 1263–1279 (2017)
17. Messikh, L., Guechi, E.H., Benloucif, M.: Critically damped stabilization of inverted-pendulum systems using continuous-time cascade linear model predictive control. J. Franklin Inst. **354**(16), 7241–7265 (2017)
18. Peker, F., et al.: *Cascade Control Approach for a Cart Inverted Pendulum System Using Controller Synthesis Method*. in 2018 *26th Mediterranean Conference on Control and Automation (MED)*. 2018. IEEE
19. Song, Y., et al.: Sliding mode variable structure control for inverted pendulum visual servo systems. IFAC-PapersOnLine **52**(11), 262–267 (2019)
20. Zhao, J., Spong, M.W.: Hybrid control for global stabilization of the cart–pendulum system. Automatica **37**(12), 1941–1951 (2001)
21. Åström, K.J.: *Hybrid control of inverted pendulums*, in *Learning, control and hybrid systems*, pp. 150–163. Springer (1999)
22. Mills, A., Wills, A., Ninness, B.. *Nonlinear model predictive control of an inverted pendulum*. in *2009 American control conference*. 2009. IEEE
23. Magni, L., Scattolini, R., Åström, K.J., *Global stabilization of the inverted pendulum using model predictive control.* IFAC Proceedings Volumes, 2002. **35**(1): p. 141–146

24. Anderson, C.W.: Learning to control an inverted pendulum using neural networks. IEEE Control Syst. Mag. **9**(3), 31–37 (1989)
25. Kuo, T., Huang, Y., Hong, B.. *Adaptive PID with sliding mode control for the rotary inverted pendulum system*. in: 2009 *IEEE/ASME International Conference on Advanced Intelligent Mechatronics*. 2009. IEEE
26. Hernández, R., Jurado, F.. *Adaptive neural sliding mode control of an inverted pendulum mounted on a ball system*. in: 2018 *15th International Conference on Electrical Engineering, Computing Science and Automatic Control (CCE)*. 2018. IEEE
27. Junior, S.S., Balthazar, J.M., Junior, B.R.P.: Non-linear dynamics of a tower orchard sprayer based on an inverted pendulum model. Biosys. Eng. **103**(4), 417–426 (2009)
28. Kimiaeifar, A., et al.: Analysis of modified Van der Pol's oscillator using He's parameter-expanding methods. Curr. Appl. Phys. **10**(1), 279–283 (2010)
29. Azimzadeh, Z., Vahidi, A., Babolian, E.: Exact solutions for non-linear Duffing's equations by He's homotopy perturbation method. Indian J. Phys. **86**(8), 721–726 (2012)
30. Zeng, D., Lee, Y.: Analysis of strongly nonlinear oscillator using the max-min approach. International Journal of Nonlinear Sciences and Numerical Simulation **10**(10), 1361–1368 (2009)
31. Pakar, I., Bayat, M.: Analytical solution for strongly nonlinear oscillation systems using energy balance method. Int. J. Phys. Sci. **6**(22), 5166–5170 (2011)
32. Pakar, I., Bayat, M., Bayat, M., *762. On the approximate analytical solution for parametrically excited nonlinear oscillators*. Journal of vibroengineering, 2012. **14**(1)
33. Sobamowo, M.: Exact Analytical Solutions of Nonlinear Differential Equation of a Large Amplitude Simple Pendulum. World Scientific News **144**, 70–88 (2020)
34. Awrejcewicz, J., Starosta, R., Sypniewska-Kamińska, G.: Asymptotic analysis of resonances in nonlinear vibrations of the 3-dof pendulum. Differential Equations and Dynamical Systems **21**(1), 123–140 (2013)
35. Ashrafiuon, H., Whitman, A.M.: *Closed-loop dynamic analysis of a rotary inverted pendulum for control design*. Journal of dynamic systems, measurement, and control, 2012. 134(2)
36. Litak, G., et al.: *Nonlinear oscillations of an elastic inverted pendulum*. in 2012 *IEEE 4th International Conference on Nonlinear Science and Complexity (NSC)*. 2012. IEEE
37. Furuta, K., Yamakita, M., Kobayashi, S., *Swing-up control of inverted pendulum using pseudo-state feedback*. Proceedings of the Institution of Mechanical Engineers, Part I: Journal of Systems and Control Engineering, 1992. **206**(4): p. 263–269

Figures

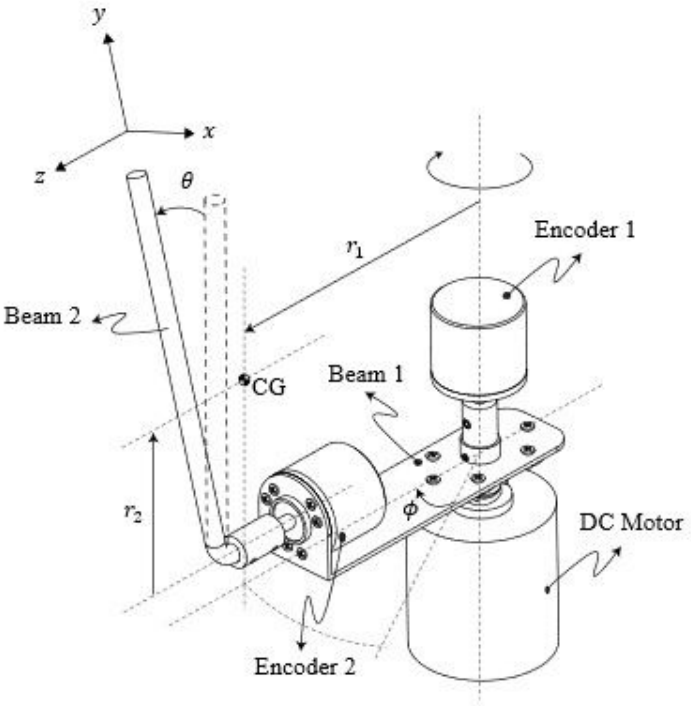

Figure 1

Schematic of the fabricated system

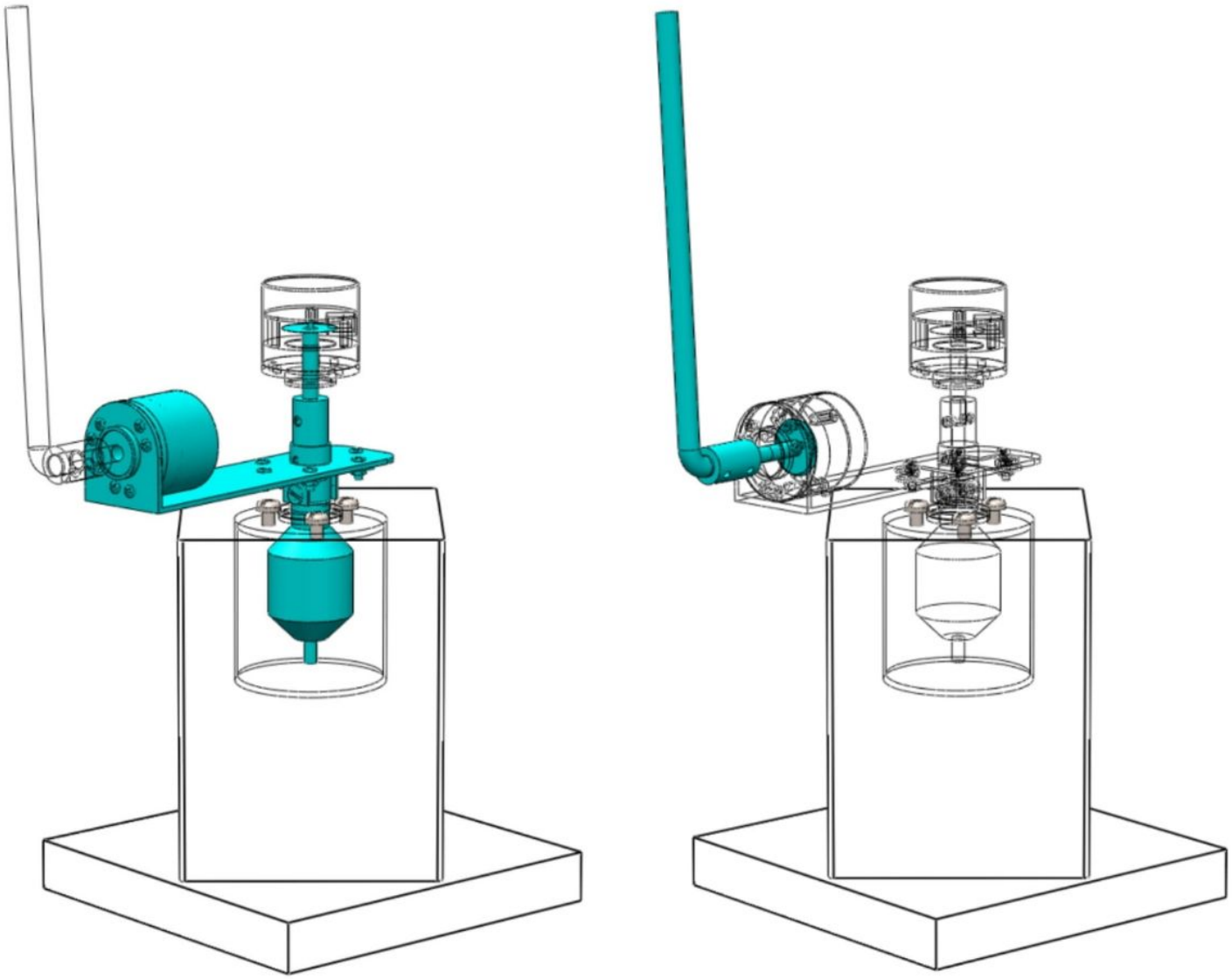

Figure 2

Different parts of the system with no relative motion forming a) rigid body 1 and b) rigid body 2

Figure 3

Photo of the experimental setup

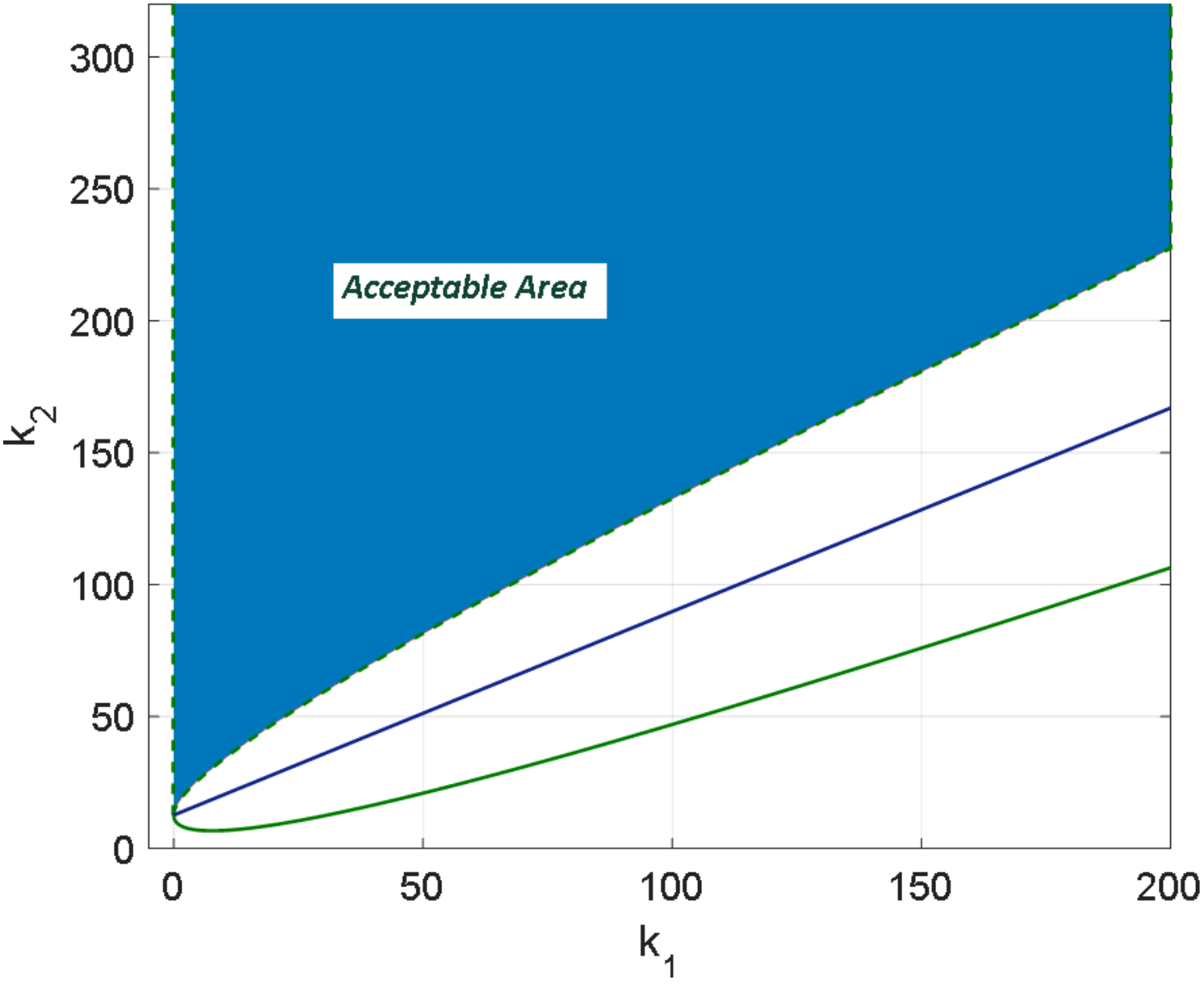

Figure 4

Acceptable area for k1 and k2

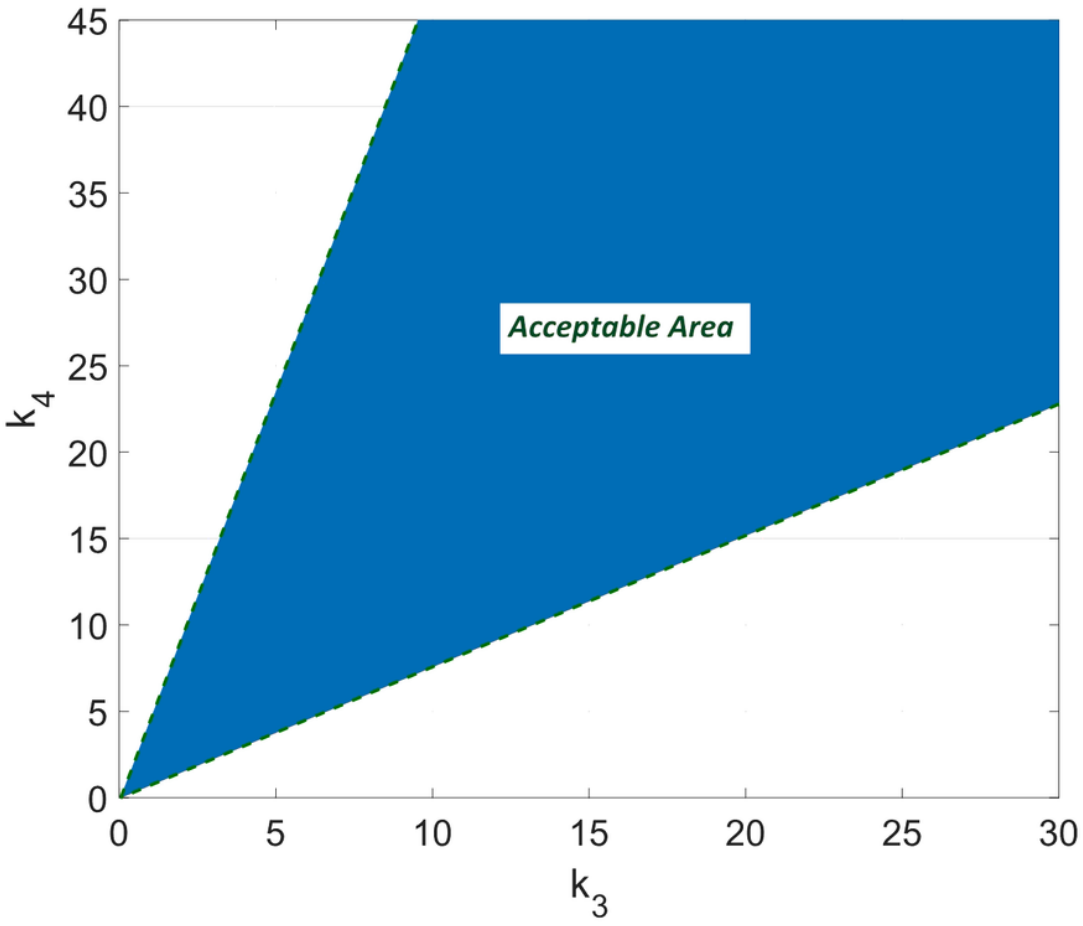

Figure 5

Acceptable area for k3 and k4

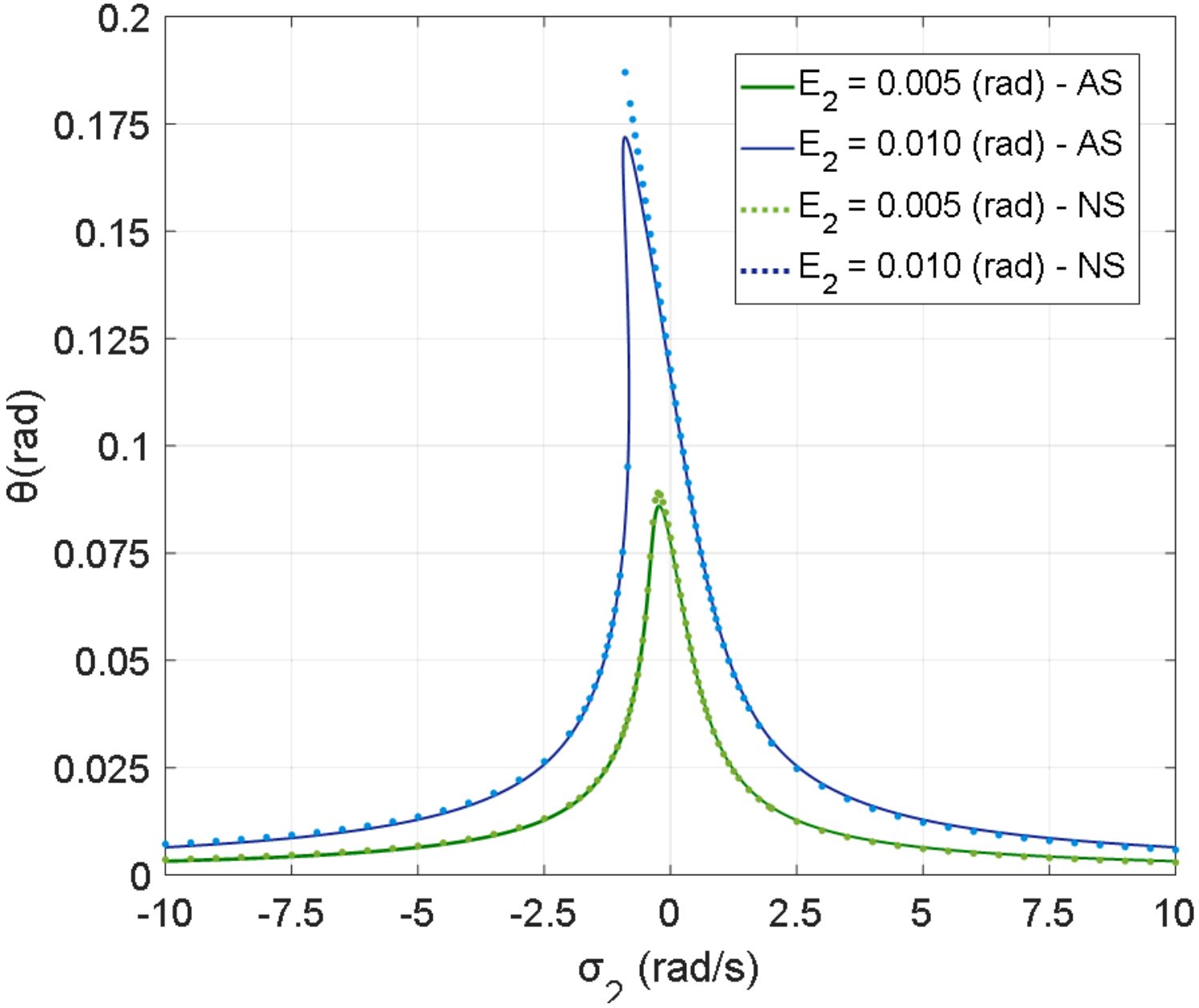

Figure 6

Nonlinear resonance phenomena for θ in the vicinity of the second natural frequency (state feedback gains: k1 = 50, k2 = 250, k3 = 0.7, k4 = 0.6) - Analytical Solution (AS) versus Numerical Solution (NS)

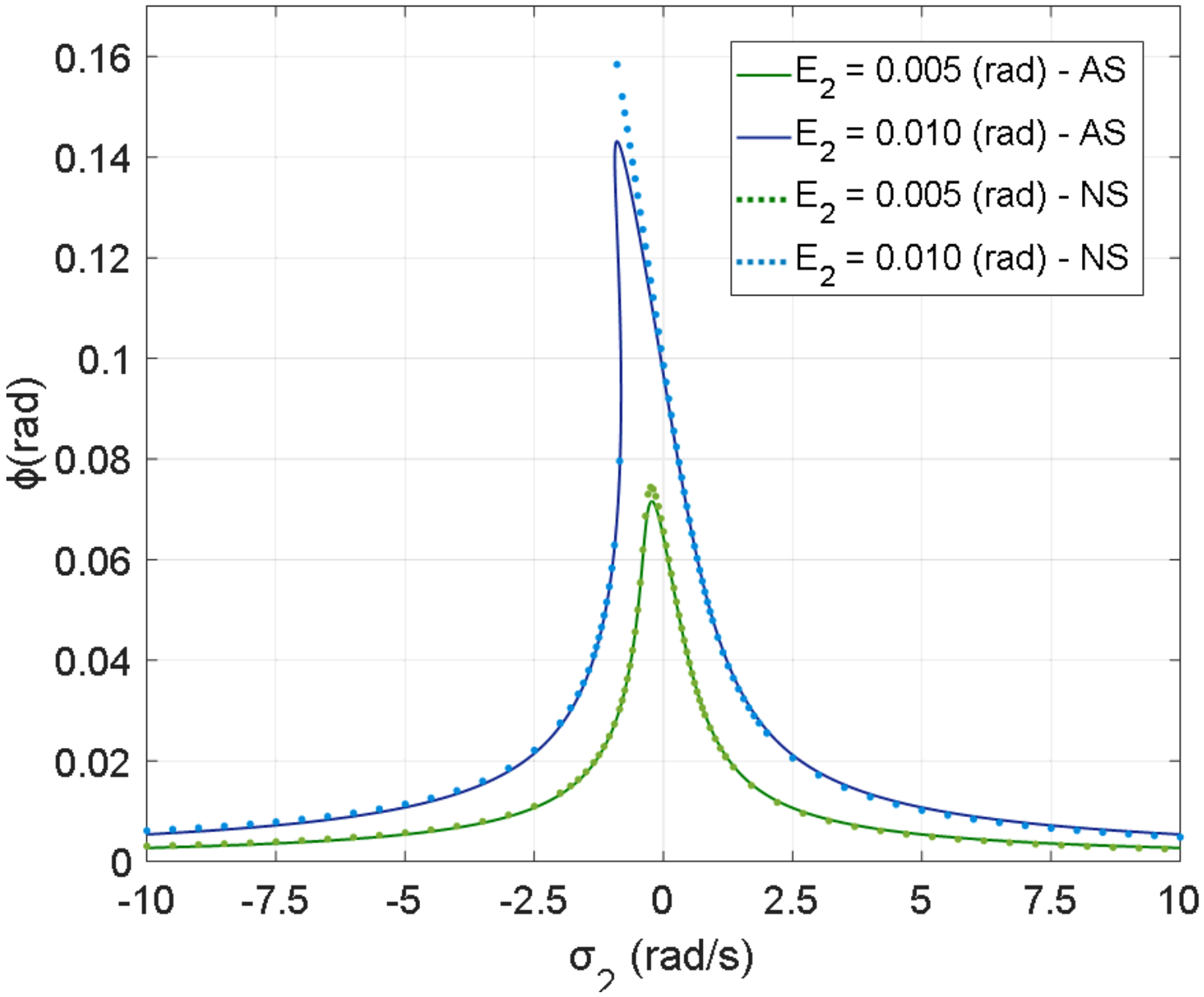

Figure 7

Nonlinear resonance phenomena for Φ in the vicinity of the second natural frequency (state feedback gains: k1 = 50, k2 = 250, k3 = 0.7, k4 = 0.6) - Analytical Solution (AS) versus Numerical Solution (NS)

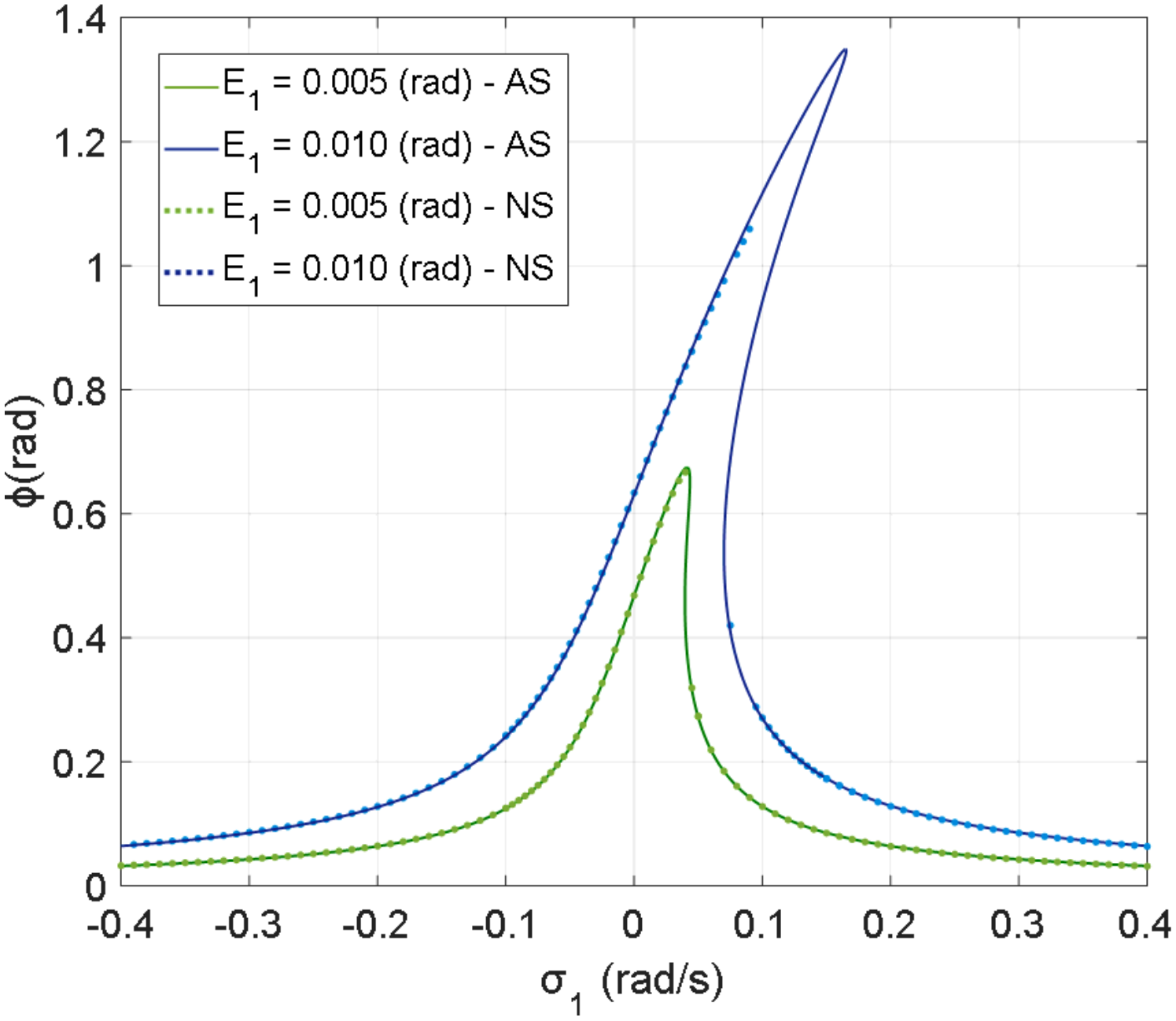

Figure 8

Nonlinear resonance phenomena for Φ in the vicinity of the first natural frequency (state feedback gains: k1 = 50, k2 = 250, k3 = 0.2, k4 = 0.3) - Analytical Solution (AS) versus Numerical Solution (NS)

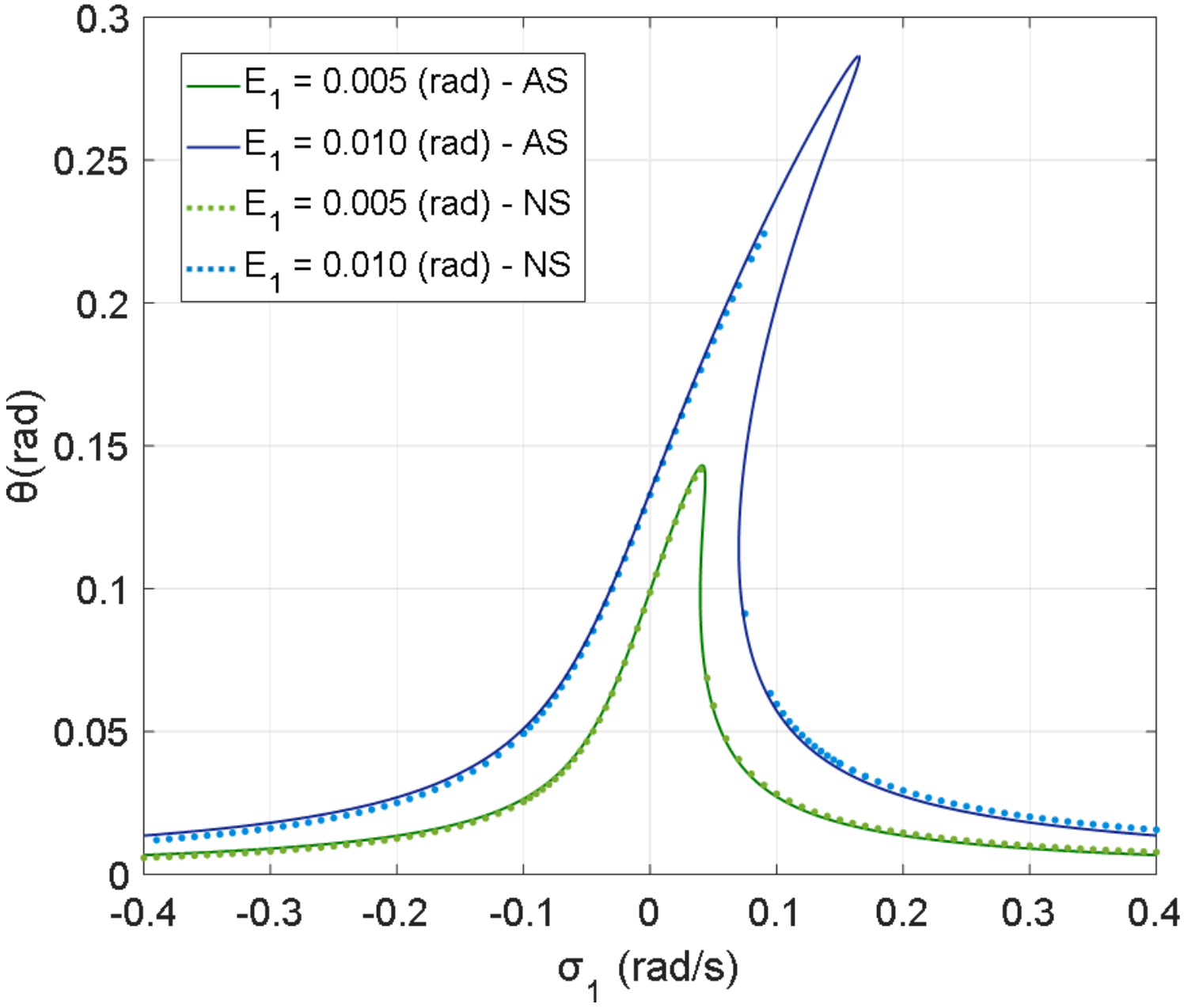

Figure 9

Nonlinear resonance phenomena for θ in the vicinity of the first natural frequency (state feedback gains: k1 = 50, k2 = 250, k3 = 0.2, k4 = 0.3) - Analytical Solution (AS) versus Numerical Solution (NS)

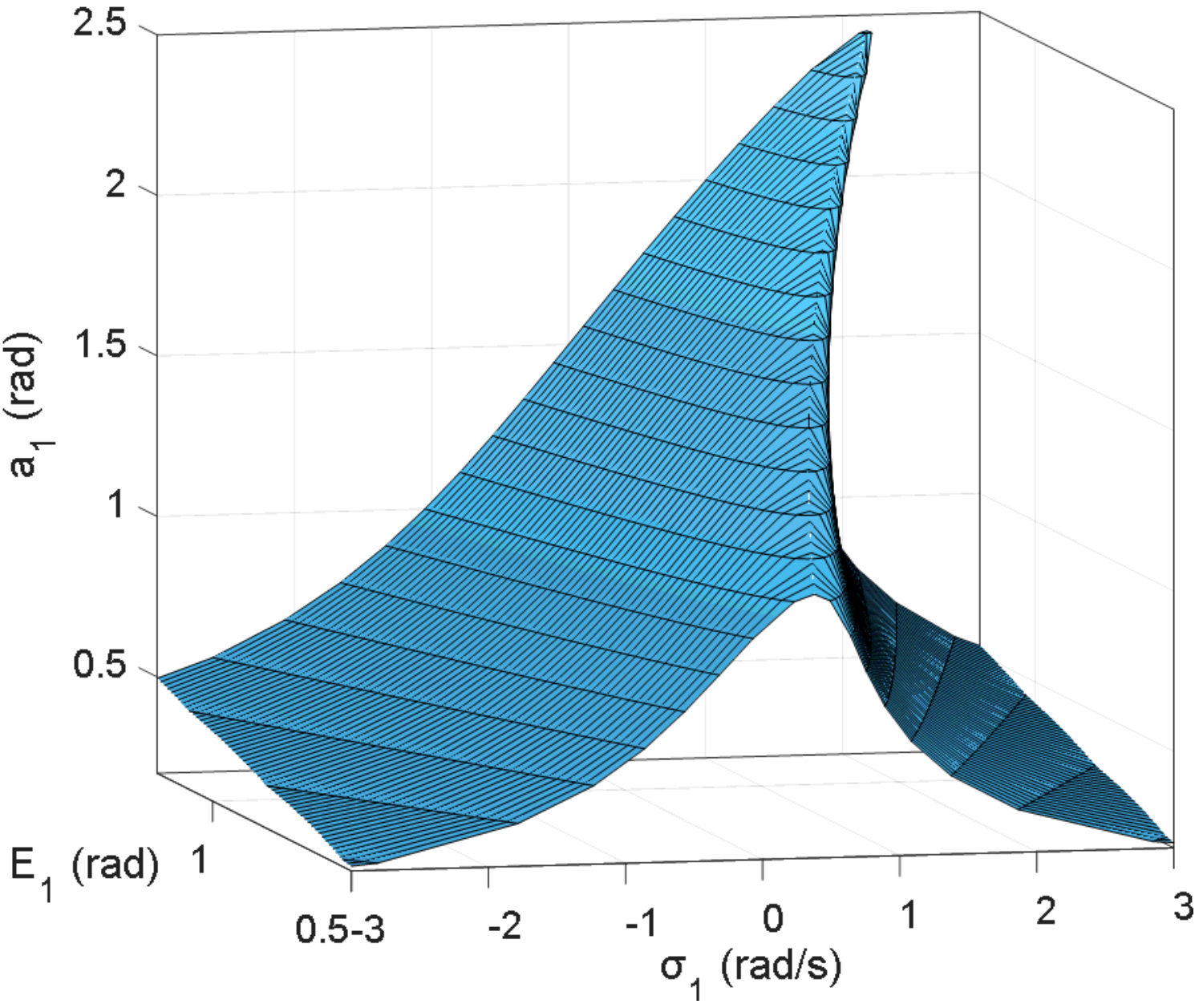

Figure 10

Vibration amplitude α1 with respect to σ1 and E1 (state feedback gains: k1 = 50, k2 = 250, k3 = 4, k4 = 12)

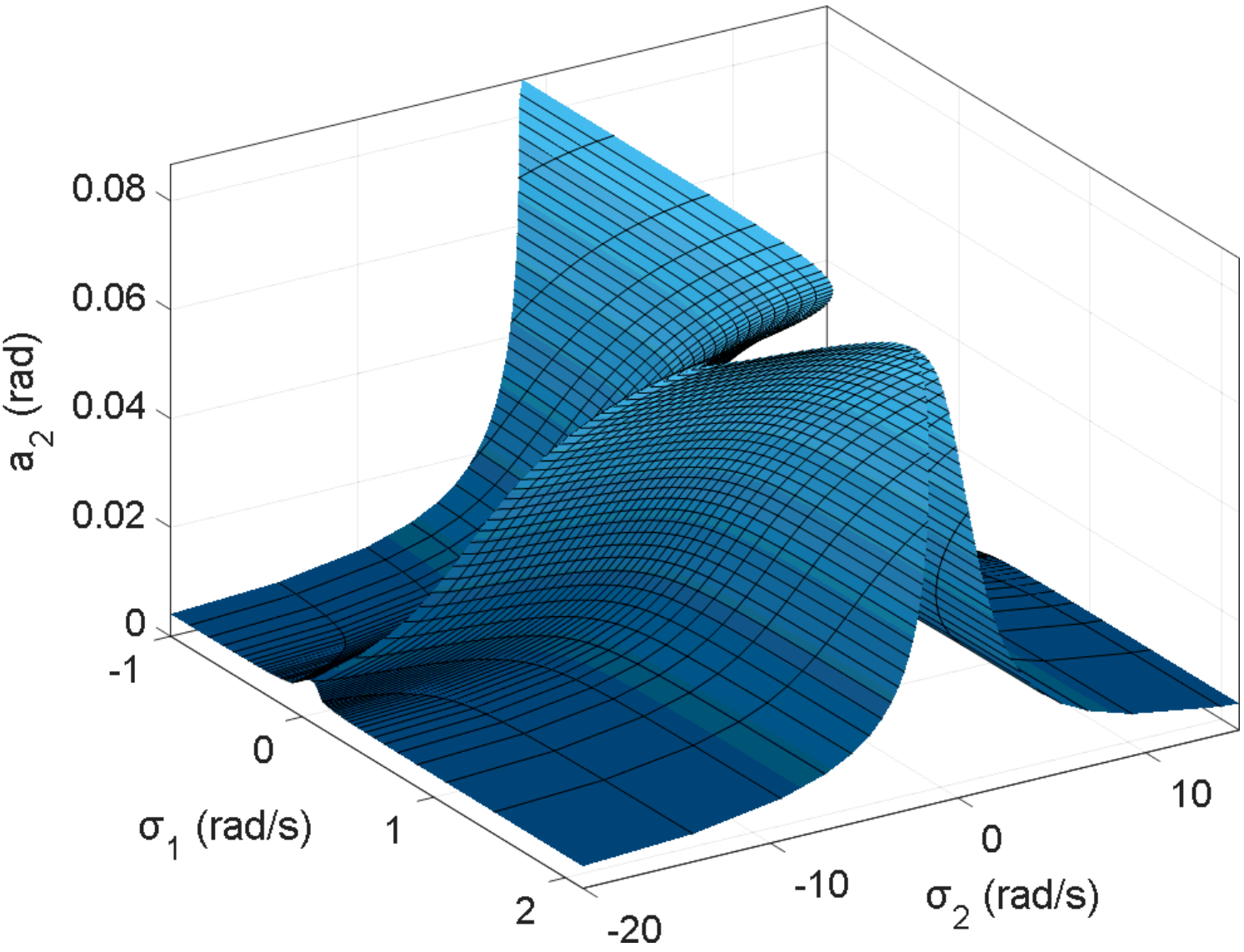

Figure 11

Vibration amplitude α2 with respect to σ1 and σ2 (state feedback gains: k1 = 50, k2 = 250, k3 = 0.8, k4 = 0.8; Excitation amplitudes: E1= 0.03 and E2 = 0.03)

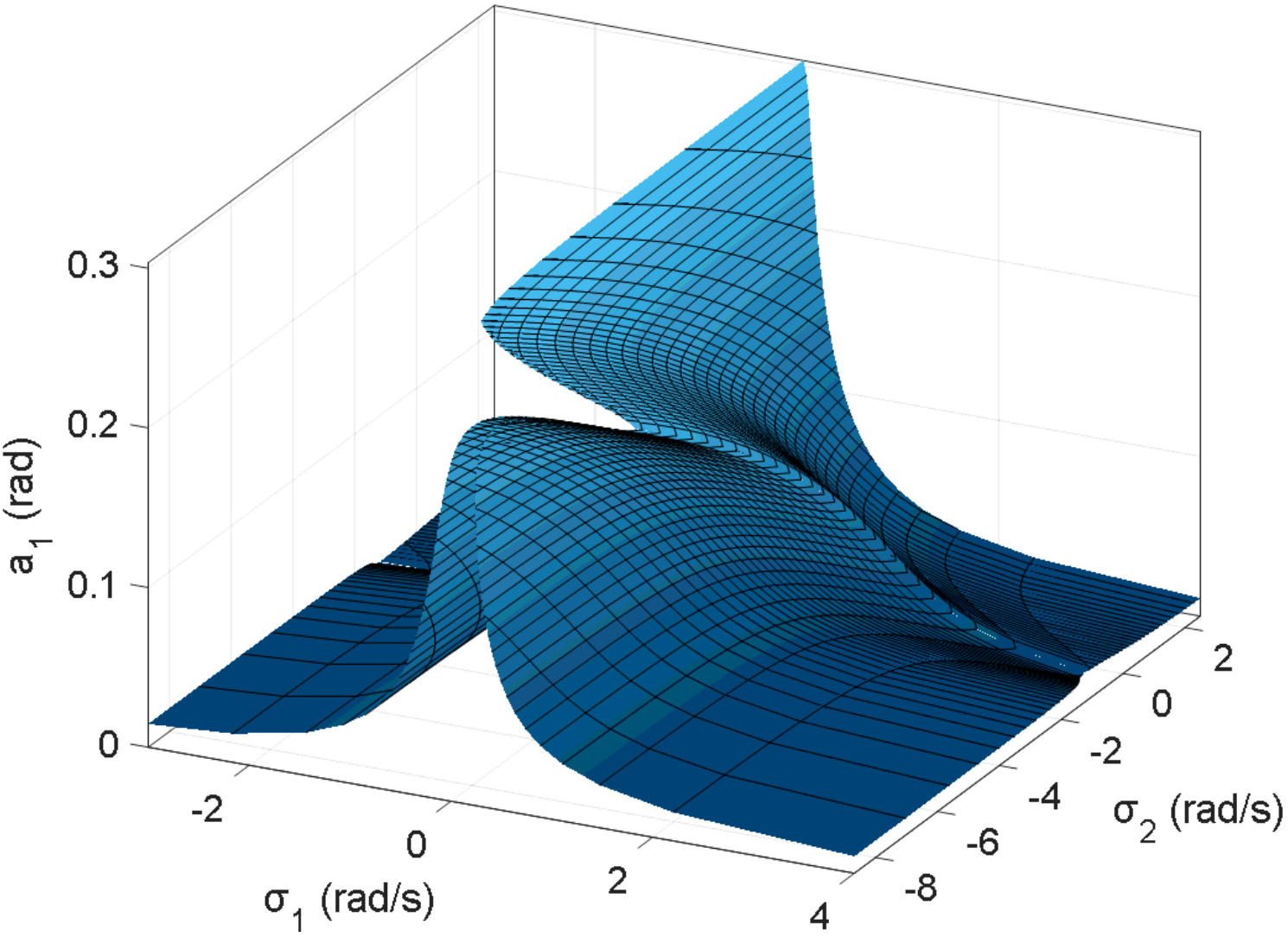

Figure 12

Vibration amplitude α1 with respect to σ1 and σ2 (state feedback gains: k1 = 50, k2 = 250, k3 = 0.8, k4 = 0.8; Excitation amplitudes: E1= 0.03 and E2 = 0.03)

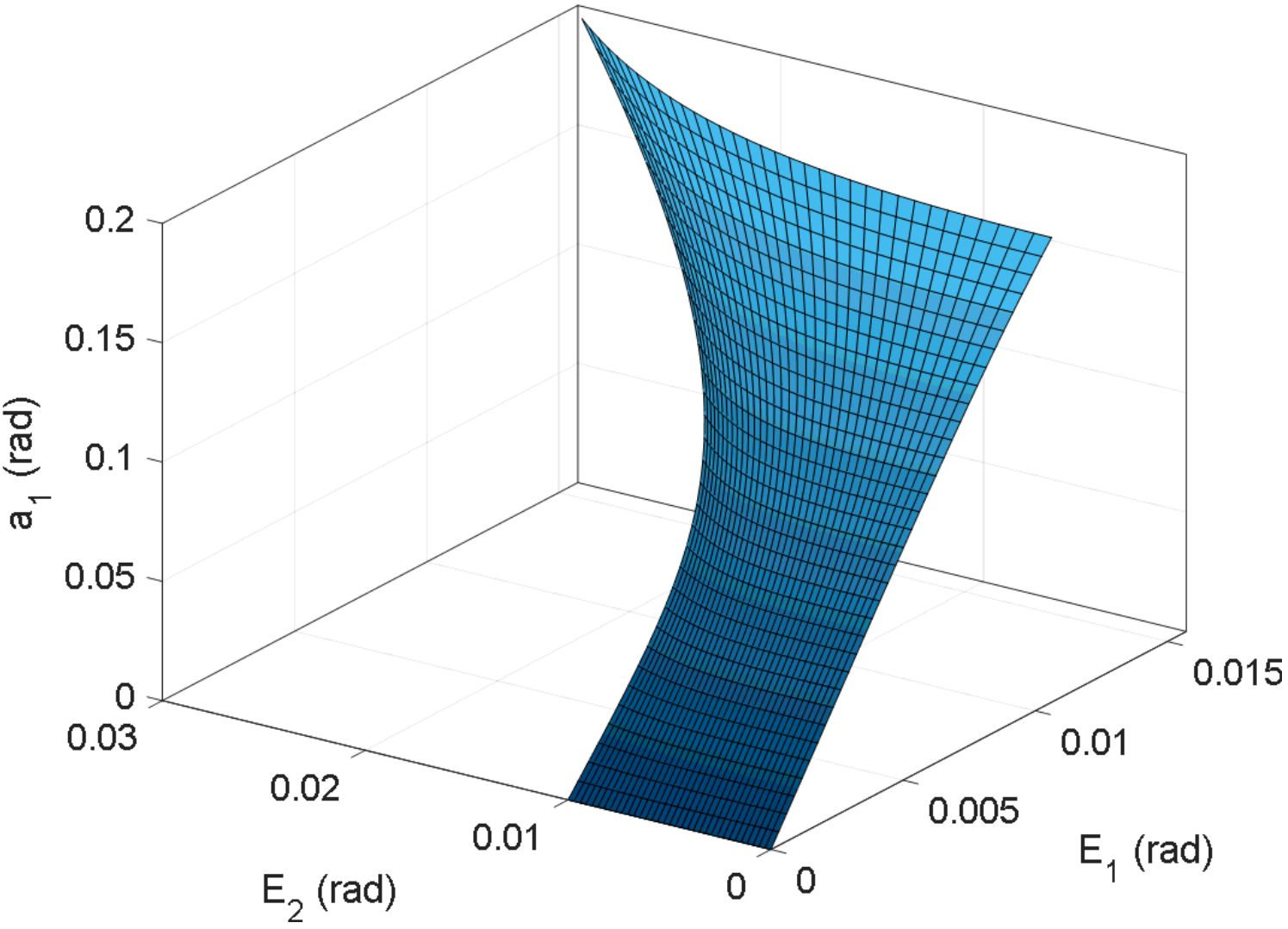

Figure 13

Vibration amplitude α1 with respect to E1 and E2 (state feedback gains: k1 = 50, k2 = 250, k3 = 0.5, k4 = 0.7; Deviations from Natural frequencies: σ1 = 0, σ2 = 0

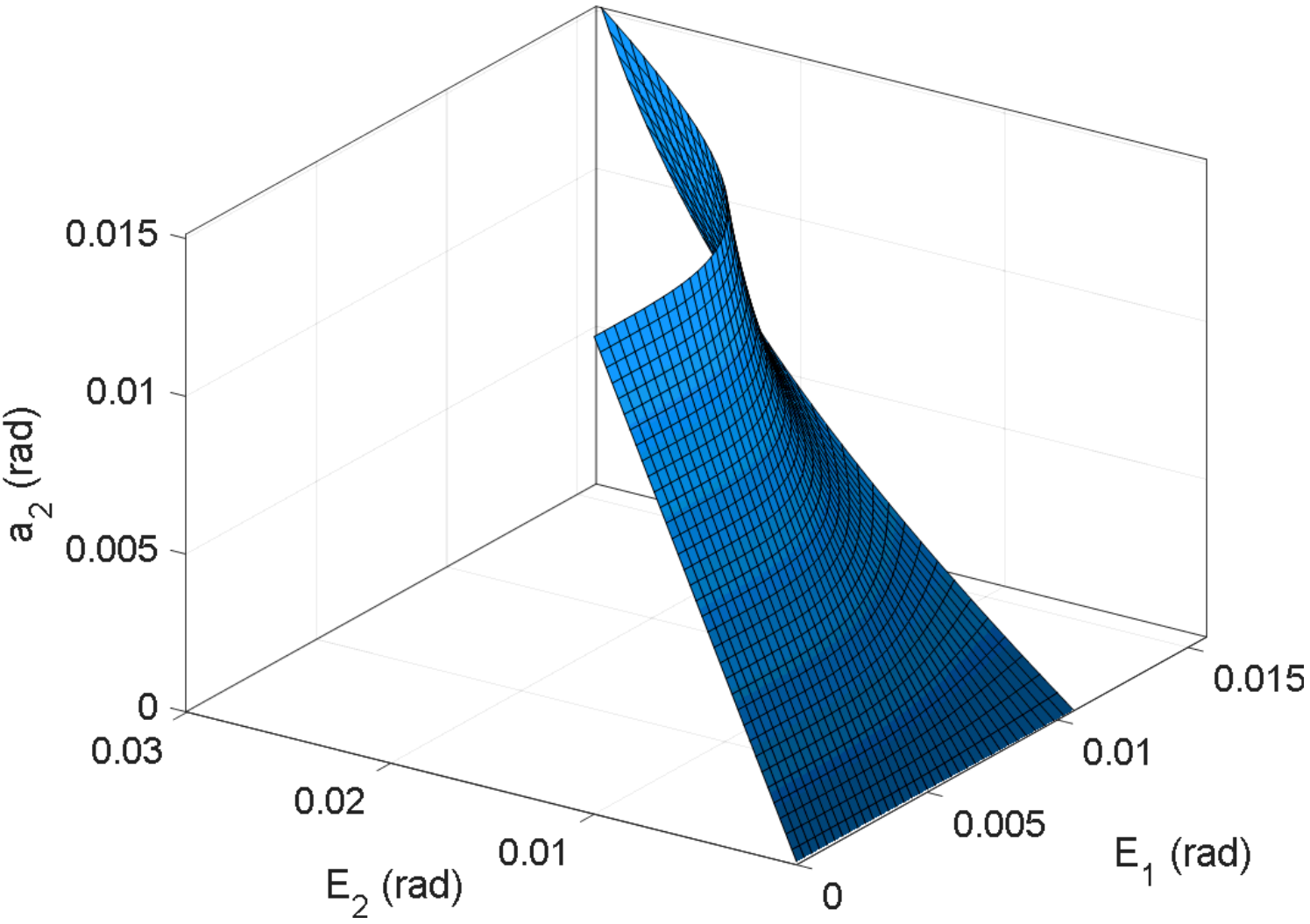

Figure 14

Vibration amplitude α2 with respect to E1 and E2 (state feedback gains: k1 = 50, k2 = 250, k3 = 0.5, k4 = 0.7; Deviations from Natural frequencies: σ1 = 0, σ2 = 0

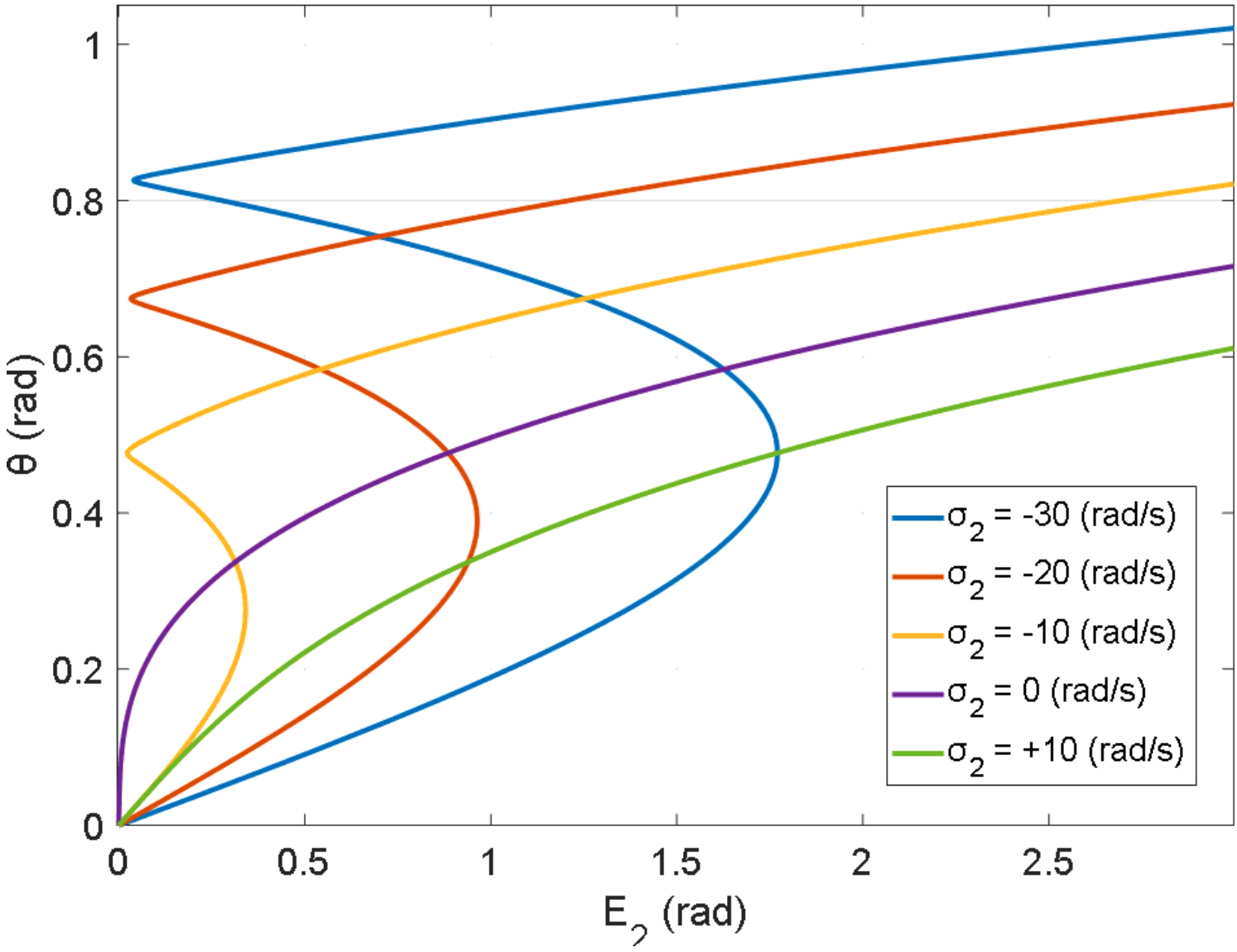

Figure 15

Amplitude of θ with respect to E2 with several values of σ2 (state feedback gains: k1 = 50, k2 = 250, k3 = 0.03, k4 = 0.25)

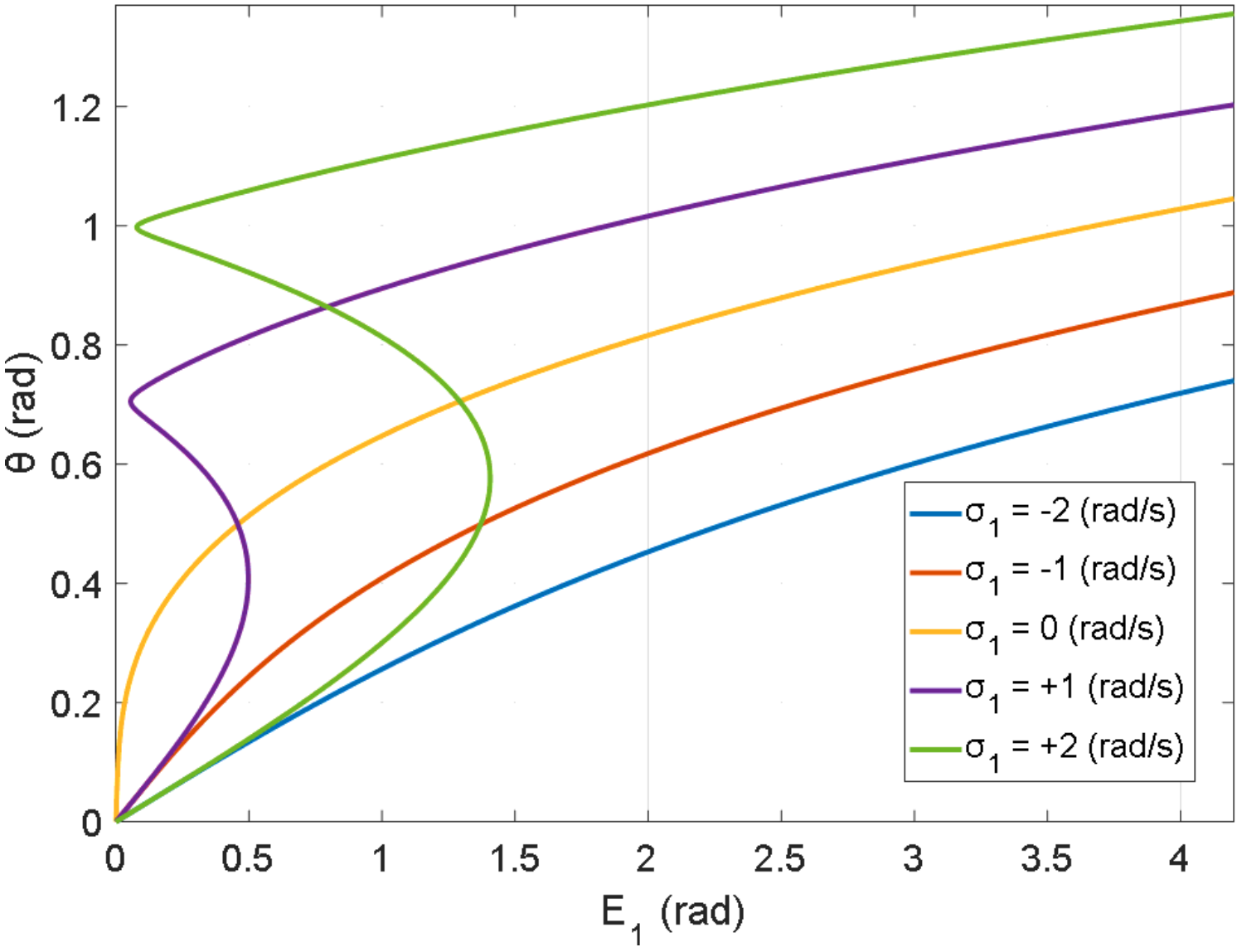

Figure 16

Amplitude of θ with respect to E1 with several values of σ1 (state feedback gains: k1 = 50, k2 = 250, k3 = 0.03, k4 = 0.25)

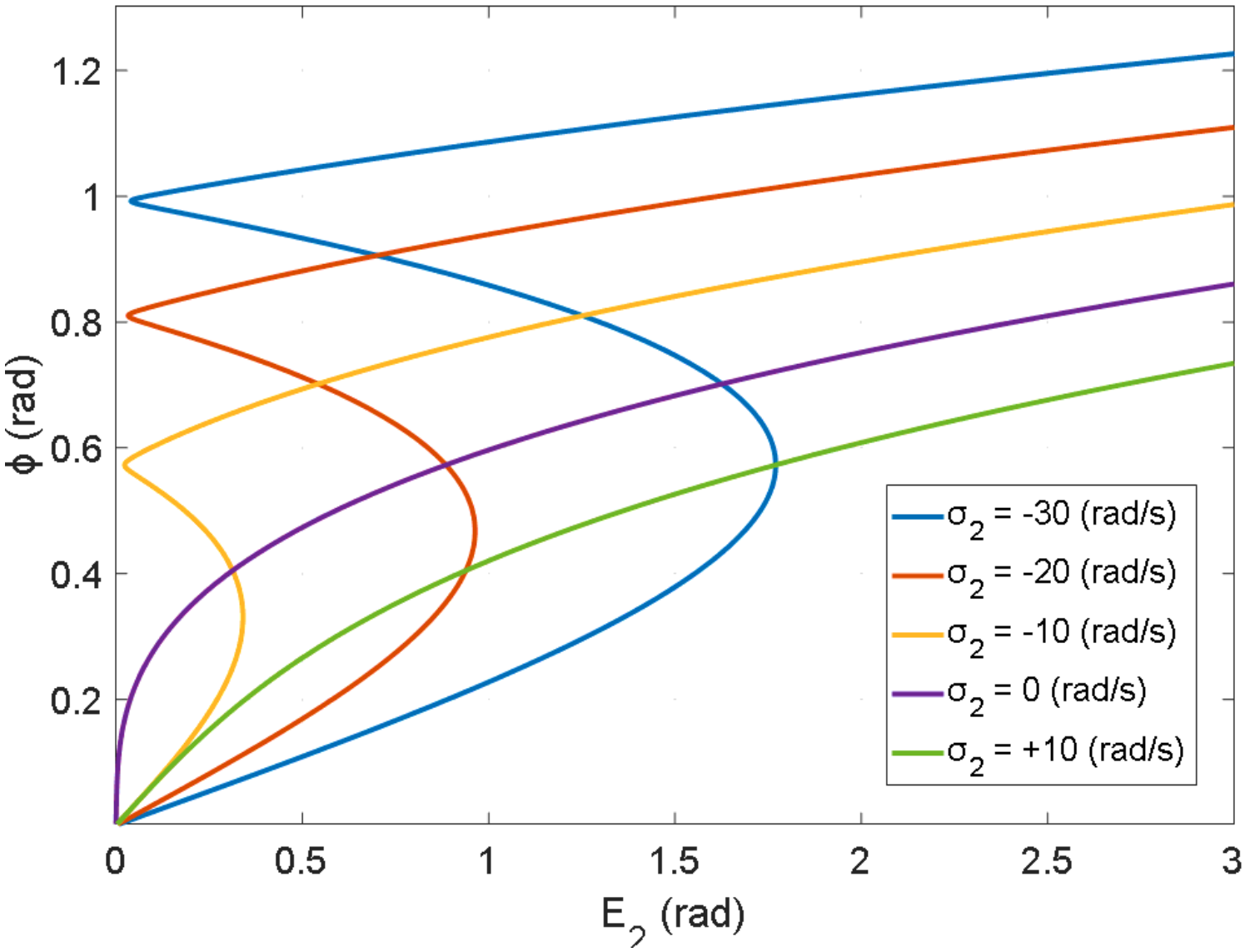

Figure 17

Amplitude of Φ with respect to E2 with several values of σ2 (state feedback gains: k1 = 50, k2 = 250, k3 = 0.03, k4 = 0.25)

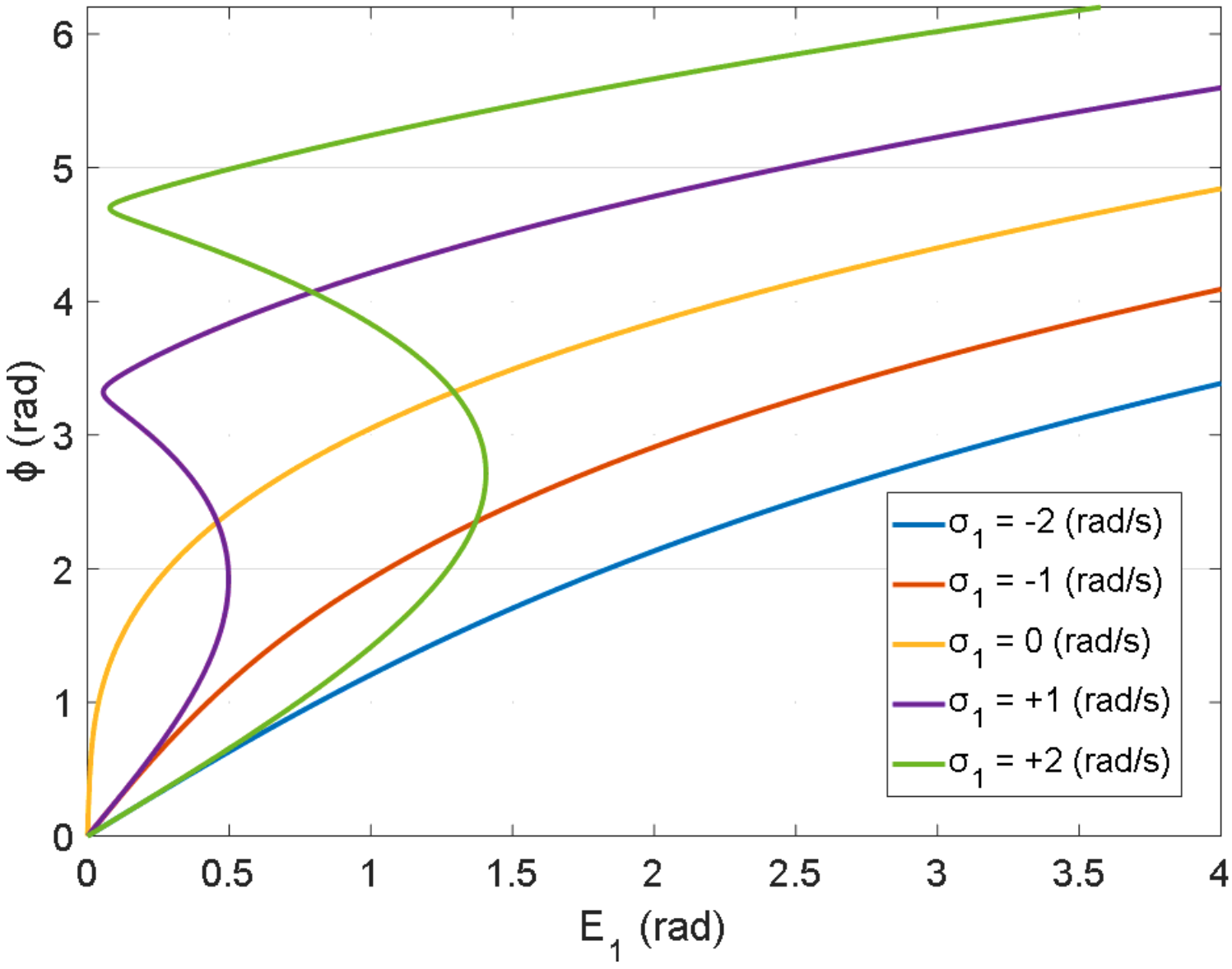

Figure 18

Amplitude of Φ with respect to E1 with several values of σ2 (state feedback gains: k1 = 50, k2 = 250, k3 = 0.03, k4 = 0.25)

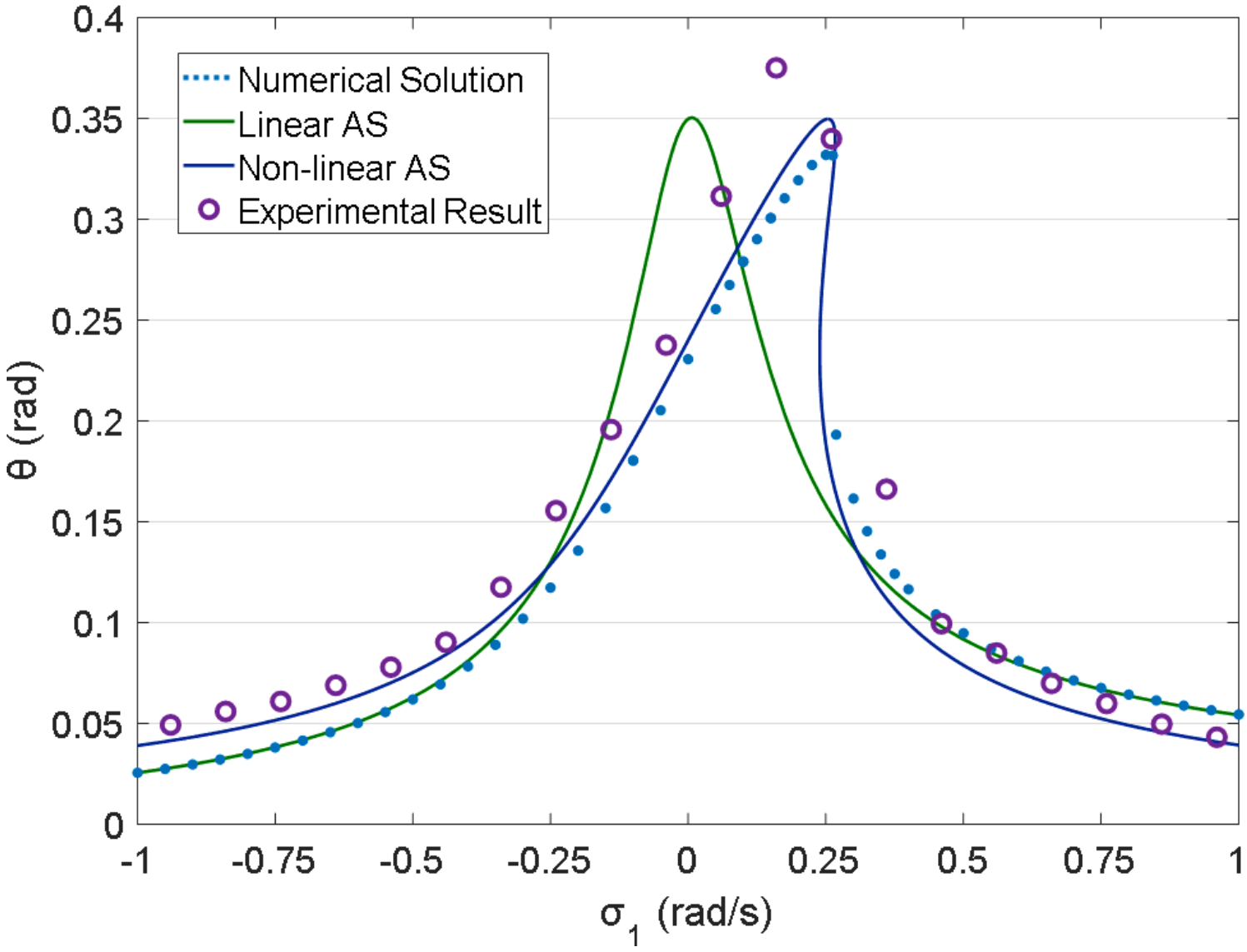

Figure 19

Verification of experimental results of θ with numerical and analytical solution in the vicinity of the first natural frequency (state feedback gains: k1 = 50, k2 = 250, k3 = 4, k4 = 10; Excitation amplitude: E1 = 0.3)

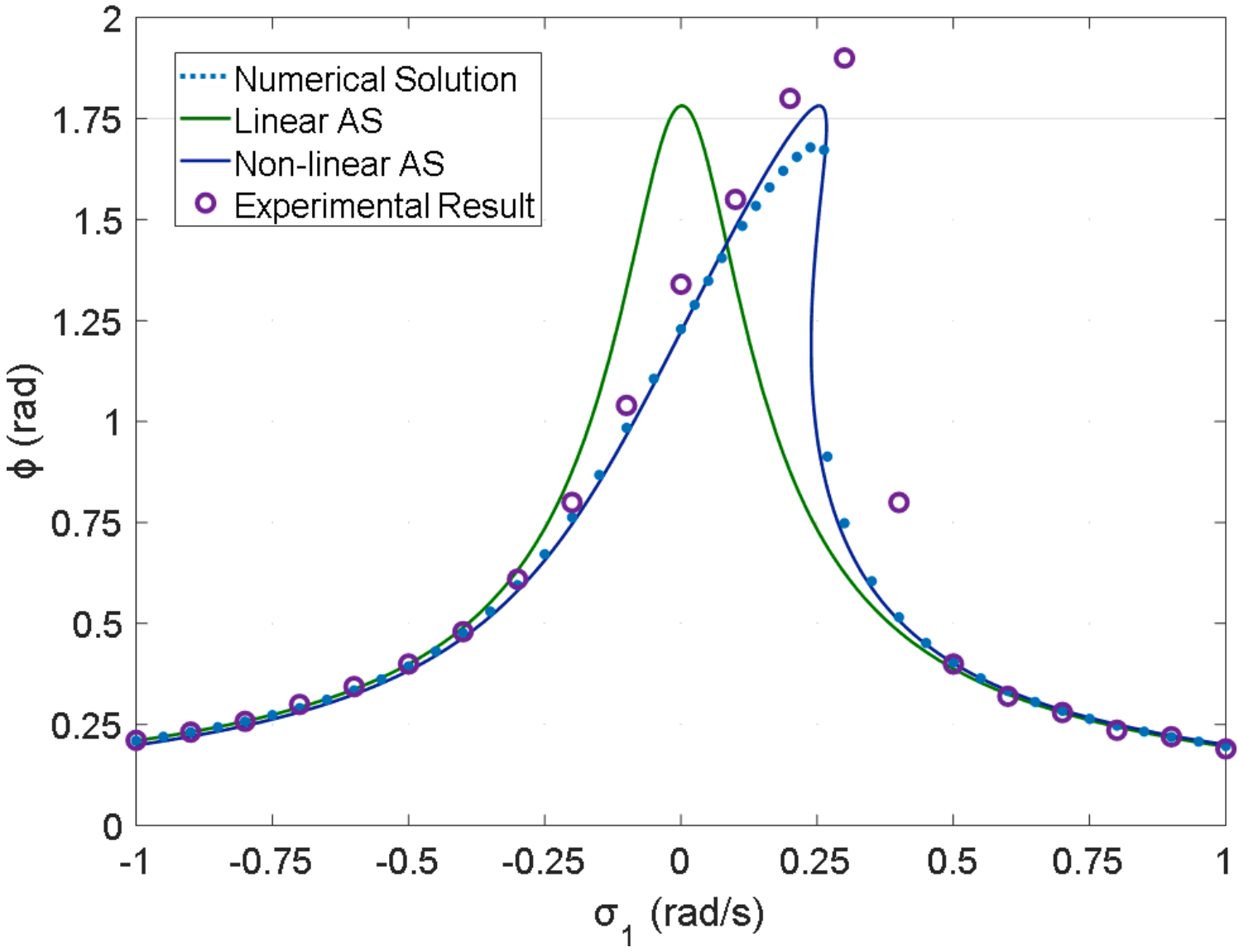

Figure 20

Verification of experimental results of Φ with numerical and analytical solution in the vicinity of the first natural frequency (state feedback gains: k1 = 50, k2 = 250, k3 = 4, k4 = 10; Excitation amplitude: E1 = 0.3)